A survey of the parallel performance and the accuracy of Poisson solvers for electronic structure calculations

Pablo García-Risueño,[*,†] Joseba Alberdi-Rodriguez,[‡] Micael J. T. Oliveira,[¶] Xavier Andrade,[§] Michael Pippig,[‖] Javier Muguerza,[‡] Agustin Arruabarrena,[‡] and Ángel Rubio[⊥]

Humboldt Universität zu Berlin and CSIC, University of the Basque Country UPV/EHU, University of Coimbra, Harvard University, Chemnitz University of Technology, and European Theoretical Spectroscopy Facility and Fritz-Haber Institut (MPG)

E-mail: risueno@physik.hu-berlin.de

Abstract

We present an analysis of different methods to calculate the classical electrostatic Hartree potential created by charge distributions. Our goal is to provide the reader with an estimation

[*]To whom correspondence should be addressed
[†]Institut für Physik, Humboldt Universität zu Berlin, 12489 Berlin, Germany - Instituto de Química Física Rocasolano (CSIC), C/ Serrano 119, 28006 Madrid, Spain
[‡]Dept. of Computer Architecture and Technology, Nano-Bio Spectroscopy Group and European Theoretical Spectroscopy Facility, Spanish node, University of the Basque Country UPV/EHU, M. Lardizabal, 1, 20018 Donostia/San Sebastián, Spain
[¶]Center for Computational Physics, University of Coimbra, Rua Larga, 3004-516 Coimbra, Portugal
[§]Dept. of Chemistry and Chemical Biology, Harvard University, 12 Oxford street, Cambridge, MA 02138, USA
[‖]Dept. of Mathematics, Chemnitz University of Technology, 09107 Chemnitz, Germany
[⊥]Nano-Bio Spectroscopy Group and European Theoretical Spectroscopy Facility, Spanish node, University of the Basque Country UPV/EHU, Edif. Joxe Mari Korta, Av. Tolosa 72, 20018 Donostia/San Sebastián, Spain - Centro de Física de Materiales, University of the Basque Country UPV/EHU, 20018 Donostia/San Sebastián, Spain - Fritz-Haber Institut der Max-Planck Gesellschaft, Faradayweg 4-6, D-14195 Berlin-Dahlem, Germany

on the performance —in terms of both numerical complexity and accuracy— of popular Poisson solvers, and to give an intuitive idea on the way these solvers operate. Highly parallelisable routines have been implemented in the first-principle simulation code OCTOPUS to be used in our tests, so that reliable conclusions about the capability of methods to tackle large systems in cluster computing can be obtained from our work.

Keywords: Hartree potential, charge density, Poisson solver, parallelisation, linear scaling, fast multipole method, parallel fast Fourier transform, interpolating scaling functions, multigrid, conjugate gradients

Contents

1 Introduction

The electrostatic interaction between charges is one of the most important phenomena of physics and chemistry, which makes the calculation of the energy and potential associated to a distribution of charges one of the most common problems in scientific computing. The calculation of potentials created by pairwise interactions is ubiquitous in atomic and molecular simulations, and also in fields like quantum chemistry, solid state physics, fluid dynamics, plasma physics, and astronomy, among others.

In particular, the electrostatic interaction is a key part in the density functional theory (DFT)[1,2] and time-dependent density functional theory (TDDFT)[3] formulations of quantum mechanics. In DFT (TDDFT) the many-body Schrödinger equation is replaced by a set of single particle equations, the Kohn–Sham (time-dependent Kohn–Sham) equations, which include an effective potential that reproduces the interelectronic interaction. Such effective potential is usually divided into three terms: Hartree potential, exchange-correlation potential and external potential. The Hartree term corresponds to the classical electrostatic potential generated by electronic charge distributions due to the (delocalised) electronic states.

The calculation of the potential associated to a charge distribution is then an important step in most numerical implementations of DFT. In addition, the calculation of the electrostatic potential associated to a charge density can appear in other contexts in electronic structure theory, like the approximation of the exchange term,[4–6] or the calculation of integrals that appear in Hartree–Fock[7,8] or Casida[9] theories. It is understandable then that the calculation of the electrostatic potential has received much interest in the recent past within the community of electronic structure researchers.

Since at present, the complexity of the problems we want to tackle requires massively parallel computational platforms,[10] every algorithm for a time-consuming task must not only be efficient in serial, but also needs to keep its efficiency when run in a very large number of parallel processes

(approximately 300,000 CPUs). The electrostatic interaction is non-local, and thus the information corresponding to different points interacting with each other can be stored in different computing units (processor cores), with a non-negligible time for data-communication among them. This makes critical the choice of the algorithm for the calculation of the Hartree potential, since as well as different accuracies, different algorithms also have different efficiencies. Thanks to the efficiency offered by the current generation of solvers, calculation of the Hartree potential usually contributes a minor fraction of the computational time of a typical DFT calculation. However, there are cases where the Poisson solver hinders the numerical performance of electronic structure calculations. For example, in parallel implementations of DFT it is common to distribute the Kohn–Sham orbitals between processors;[11] for real-time TDDFT in particular, this is a very efficient strategy.[12–14] Nonetheless, since a single Poisson equation needs to be solved independently on the number of orbitals, the calculation of the Hartree potential becomes an important bottleneck for an efficient parallelisation[14,15] as predicted by Amdahl's law,[16] if it is not optimally parallelised.

The objective of this article is, therefore, to analyse the relative efficiencies and accuracies of some of the most popular methods to calculate the Hartree potential created by charge distributions. Our purpose is to provide the reader with estimates on the features of this solvers that make it possible to choose which of them is the most appropriate for his electronic structure calculations.

We start by giving a brief theoretical introduction to the Poisson equation problem and on different methods to solve it. Next, we discuss the details of our implementation and the parallel computers we use. Following, we present the results of our numerical experiments. We finish by stating our conclusions. More specific derivations and analysis are provided in the supporting info.

2 Theoretical background

In the context of quantum mechanics, the electrons and their electric charge are delocalised over space forming a continuous charge distribution $\rho(\boldsymbol{r})$. Such a charge density creates an electrostatic

potential $v(\boldsymbol{r})$, which is given by[17]

$$v(\boldsymbol{r}) = \int d\boldsymbol{r}\,' \frac{1}{4\pi\varepsilon_0} \frac{\rho(\boldsymbol{r}\,')}{|\boldsymbol{r}-\boldsymbol{r}\,'|} \,, \tag{1}$$

where ε_0 is the electrical permittivity of the vacuum, i.e. $1/4\pi$ in atomic units. When considering the electric interaction in a medium, it is possible to approximate the polarization effects by replacing ε_0 by an effective permittivity, ε. In the context of electronic structure calculations this effective permittivity is used, for example, in multiscale simulations where part of the system is approximated by a continuous polarisable medium.[18]

In 3D, it is simple to show that equation Eq. (1) is equivalent to the Poisson equation[19,20]

$$\nabla^2 v(\boldsymbol{r}) + \frac{\rho(\boldsymbol{r})}{\varepsilon_0} = 0 \,. \tag{2}$$

In fact, this equation provides a convenient general expression that is valid for different dimensions and boundary conditions. For example, to study crystalline systems, usually periodic boundary conditions are imposed. It is also possible to simulate a molecular system interacting with ideal metallic surfaces by choosing the appropriate boundary conditions.[21,22] Both formulations of the problem, i.e. equations Eq. (1) and Eq. (2), are quite useful: while some methods to calculate the Hartree potential are based on the former, others rely on the latter.

In order to numerically calculate the electrostatic potential we need to discretise the problem. To this end, we use a grid representation, which changes the charge density and the electrostatic potential to discrete functions, with values defined over a finite number of points distributed over a uniform mesh. Such an approach is used in many electronic structure codes, even when another type of discretisation is used for the orbitals. There are several ways to calculate the potential in a grid-based approach. Probably the simplest method is to approximate equation Eq. (1) as a sum over grid points; this approximation, however, can produce large errors, and some correction terms need to be considered (this is discussed in section Section 2.3). Other methods to calculate the potential on a mesh can be found using Fourier transforms or finite differences and are based on a

discretisation of the Poisson equation.

Independently of the method, the direct calculation of the potential would take $\mathcal{O}(N^2)$ operations, with N the number of points of our grid. This is prohibitive for systems beyond some size. Fortunately, there exist a variety of methods that, by exploiting the properties of the problem, reduce the cost to a linear or quasi-linear dependency. For our survey, we have selected several parallel implementations of some of the most popular of these methods (parallel fast Fourier transform, interpolating scaling functions, fast multipole method, conjugate gradients, and multigrid). In the next subsections we introduce them and give a brief account of their theoretical foundations and properties.

2.1 Parallel fast Fourier transform (PFFT)

The Fourier transform (FT) is a powerful mathematical tool both for analytical and numerical calculations, and certainly it can be used to calculate the electrostatic potential created by a charge distribution represented in an equispaced grid by operating as follows. Let $\hat{f}(\boldsymbol{k})$ be the Fourier transform of the $f(\boldsymbol{r})$ function, and $\hat{g}^{-1}(\boldsymbol{r})$ the inverse Fourier transform of the $g(\boldsymbol{k})$ function, with f and g continuous functions defined in a tridimensional space. By construction, $f = f(\boldsymbol{r})$. The convolution property of the Fourier transform ensures that $\hat{f}^{-1}\big(\hat{f}(\boldsymbol{k})\big)(\boldsymbol{r}) = f(\boldsymbol{r})$. If we apply these equations to equation Eq. (1), we find that

$$v(\boldsymbol{r}) = \hat{v}^{-1}\big(\hat{v}(\boldsymbol{k})\big)(\boldsymbol{r}) = \frac{1}{4\pi\varepsilon_0}\hat{v}^{-1}\big(\hat{\rho}(\boldsymbol{k})/|\boldsymbol{k}|^2\big)\ , \tag{3}$$

where we have used that the Fourier transform of the function $1/|\boldsymbol{r}|$ is[20] $(\widehat{1/|\boldsymbol{r}|})(\boldsymbol{k}) = 1/|\boldsymbol{k}|^2 = 1/(k_x^2+k_y^2+k_z^2)$.

Since $\rho(\boldsymbol{r})$ is represented in discrete equispaced points $(r_{j,k,l})$ at the centre of cells whose volume equals Ω, the Fourier transform of $\rho(\boldsymbol{r})$ (i.e. $\hat{\rho}(\boldsymbol{k})$) can be calculated using its discrete

Fourier transform (i.e., the last term in the next equation):

$$\hat{\rho}(\boldsymbol{k}) := (2\pi)^{-3/2} \int d\boldsymbol{r}\, exp(-i\boldsymbol{k}\cdot\boldsymbol{r})\rho(\boldsymbol{r}) \tag{4}$$

$$\simeq (2\pi)^{-3/2}\Omega \sum_{j,k,l} \rho(r_{j,k,l}) exp(-i(k_x j + k_y k + k_z l)) \; . \tag{5}$$

The use of equation Eq. (3) in equation Eq. (3) results in a discretised problem, which requires the use of a discrete Fourier transform plus an inverse discrete Fourier transform. The expression of the potential in terms of discrete Fourier transforms makes possible the employ of the efficient technique FFT[23] (see below for details), so the problem can be sovled in $\mathcal{O}(Nlog_2 N)$ steps, N being the total number of grid points.

It is to be stressed that the use of the FT automatically imposes periodic boundary conditions on the density, and therefore to the potential. When finite systems are studied some scheme is required to avoid the interaction between periodic images. The simplest strategy is to increase the size of the real-space simulation cell and set the charge density to zero in the new points. This moves the periodic replicas of the density away, thus decreasing their effect on the potential. Another strategy is to replace the $1/(\varepsilon_0 \boldsymbol{k}^2)$ factor of equation Eq. (3), known as the kernel of the Poisson equation, by a quantity that gives the free space potential in the simulation region. This modified kernel has been presented in references [24] for molecules, one-dimensional systems, and slabs. This Coulomb cut-off technique is very efficient and easy to implement. In our PFFT-based solver we combine the two approaches, doubling the size of the cell and using a modified kernel.[20,24] This results in a potential that accurately reproduces the free space results.

In one dimension, the discrete Fourier transform of a set of n complex numbers f_k (f_k can be, for example, the values of ρ in a set of discrete points) is given by

$$F_l = \sum_{k=0}^{n-1} f_k \exp\left(-2\pi i \tfrac{kl}{n}\right) \qquad \text{for } l = 0, \ldots, n-1 \; , \tag{6}$$

with i being the imaginary unit. The inverse discrete Fourier transform is given by

$$f_k = \frac{1}{n} \sum_{l=0}^{n-1} F_l \exp\left(+2\pi i \tfrac{kl}{n}\right) \qquad \text{for } k = 0, \ldots, n-1 \ . \tag{7}$$

The definitions above enable computational savings using the fact that both the input and output data sets ($\rho(\boldsymbol{r})$ and $v(\boldsymbol{r})$) are real. Thus $F_{n-l} = F_l^*$, and in one direction we just need to calculate one half of the n discrete Fourier transforms.

The Poisson problem using equations Eq. (6) and Eq. (7) would require $\mathcal{O}(N^2)$ arithmetic operations (with e.g. $N = n^3$), which would not represent any improvement over the cost of evaluating the potential directly. However, in 1965, J. W. Cooley and J. W. Tukey published an algorithm called fast Fourier transform (FFT)[23] that exploits the special structure of equation Eq. (6) in order to reduce the arithmetic complexity. The basic idea of the radix-2 Cooley-Tukey FFT is to split a discrete FT of even size $n = 2m$ into two discrete FTs of half the length; e.g., for $l = 0, \ldots, m-1$ we have

$$\begin{aligned} F_{2l} &= \sum_{k=0}^{m-1} f_k \exp\left(-2\pi i \tfrac{k2l}{n}\right) + f_{k+m} \exp\left(-2\pi i \tfrac{(k+m)2l}{n}\right) \\ &= \sum_{k=0}^{m-1} (f_k + f_{k+m}) \exp\left(-2\pi i \tfrac{kl}{m}\right) \ ; \end{aligned} \tag{8}$$

$$\begin{aligned} F_{2l+1} &= \sum_{k=0}^{m-1} f_k \exp\left(-2\pi i \tfrac{k(2l+1)}{n}\right) + f_{k+m} \exp\left(-2\pi i \tfrac{(k+m)(2l+1)}{n}\right) \\ &= \sum_{k=0}^{m-1} \exp\left(-2\pi i \tfrac{k}{n}\right) (f_k - f_{k+m}) \exp\left(-2\pi i \tfrac{kl}{m}\right) \ . \end{aligned} \tag{9}$$

If we assume n to be a power of two, we can apply this splitting recursively $\log_2 n$ times, which leads to $\mathcal{O}(n \log_2 n)$ arithmetic operations for the calculation of equation Eq. (6). There exist analogous splitting for every divisible sizes,[25] even for prime sizes.[26]

In three dimensions a discrete FT of size $n_1 \times n_2 \times n_3$ can be evaluated using 1D FFTs along each direction, yielding a fast algorithm with arithmetic complexity $\mathcal{O}(n_1 n_2 n_3 \log(n_1 n_2 n_3))$. In addition, the one-dimensional decomposition of the 3D-FFT provides a straightforward parallelisa-

tion strategy based on a domain decomposition strategy. We now present the two-dimensional data decomposition that was first proposed by H. Q. Ding *et al.*[27] and later implemented by M. Eleftheriou *et al.*[28–30]

The starting point is to decompose the input data set along the first two dimensions into equal blocks of size $\frac{n_1}{P_1} \times \frac{n_2}{P_2} \times n_3$ and distribute these blocks on a two-dimensional grid of $P_1 \times P_2$ processes. Therefore, each process can perform $\frac{n_1}{P_1} \times \frac{n_2}{P_2}$ one-dimensional FFTs of size n_3 locally. Afterwards, a communication step is performed that redistributes the data along directions 1 and 3 in blocks of size $\frac{n_1}{P_1} \times n_2 \times \frac{n_3}{P_2}$, such that the 1D-FFT along direction 2 can be performed locally on each process. Then, a second communication step is performed, that redistributes the data along direction 2 and 3 in blocks of size $n_1 \times \frac{n_2}{P_1} \times \frac{n_3}{P_2}$. Now, the 3D-FFT is completed by performing the 1D-FFTs along direction 1. This algorithm is illustrated in Figure 1. For $n_1 \geq n_2 \geq n_3$ the two-dimensional data decomposition allows the usage of at most $n_2 \times n_3$ processes.

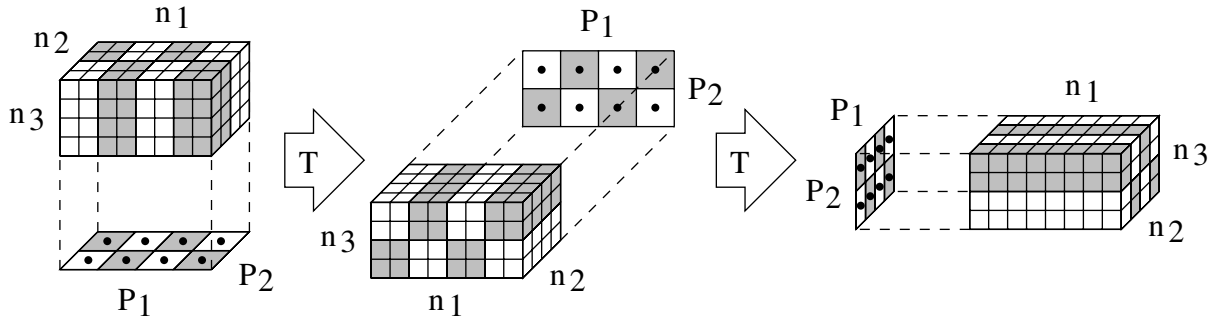

Figure 1: Distribution of a three-dimensional dataset of size $n_1 \times n_2 \times n_3 = 8 \times 4 \times 4$ on a two-dimensional process grid of size $P_1 \times P_2 = 4 \times 2$.

Since it is not trivial to implement an efficient FFT routine in parallel, we rely on optimised implementations .[31–33] Fortunately, several publicly available FFT software libraries are available that are based on the two-dimensional data decomposition. Among them are the FFT package from Sandia National Laboratories,[34] the P3DFFT software library,[35] the 2DECOMP&FFT package,[36] and the PFFT software library.[31–33] Other efficient implementations exist, but unfortunately they are not distributed as stand-alone packages.[37] Our test runs are implemented with the help of the PFFT software library,[33] which utilises the FFTW[38] software package for the one-dimensional FFTs and the global communication steps. PFFT has a similar performance to the well-known

P3DFFT, as well as some user-interface advantages,[32] so we choose it for our survey.

2.2 Fast Fourier transform with interpolating scaling functions (ISF)

This a different solver based on the Fourier approach. It was developed by Genovese *et al.*[39] for the BIGDFT code.[40] Formally this solver is based on representing the density in a basis of interpolating scaling functions (ISF) that arise in the context of wavelet theory.[41] A representation of ρ from $\rho_{j,k,l}$ can be efficiently built by using wavelets, and efficient iterative solvers for the Hartree potential v can be taylored, e.g. from ordinary steepest descent or conjugate gradient techniques.[42] A non-iterative and accurate way to calculate v[39] is to use the fast Fourier transform (FFT) in addition to wavelets. If we represent

$$\rho(\boldsymbol{r}) = \sum_{j,k,l} \rho_{j,k,l} \phi(x-j)\phi(y-k)\phi(z-l) \ , \tag{10}$$

where $\boldsymbol{r} = x,y,z$ and ϕ are interpolating scaling functions in one dimension, then equation Eq. (1) becomes

$$v_{m,n,o} = \sum_{j,k,l} \rho_{j,k,l} K(j,m;k,n;l,o) \ , \tag{11}$$

where

$$K(j,m;k,n;l,o) := \int_V d\boldsymbol{r}\,' \frac{\phi_j(x')\phi_k(y')\phi_l(z')}{|\boldsymbol{r}-\boldsymbol{r}\,'|} \ , \tag{12}$$

and V indicates the total volume of the system. Due to the definition of the ISF, the discrete kernel K satisfies $K(j,m;k,n;l,o) = K(j-m;k-n;l-o)$, and therefore equation Eq. (11) is a convolution, which can be efficiently treated using FFTs (see the previous section). The evaluation of equation Eq. (12) can be approximated by expressing the inverse of r in a Gaussian basis ($1/r \simeq \sum_k \omega_k \exp(-p_k r^2)$), which also enables efficient treatment. All this makes the order of this method $N\log_2(N)$.

This method is nearly equivalent to the scheme presented in the previous section. ISF's main

characteristic is that it uses a kernel in equation Eq. (3) that yields an accurate free space potential without having to enlarge the cell. For the purposes of the discussion below we consider it a different solver since it is distributed as a standalone package that includes its own parallel FFT routine,[42] so it has different scaling properties than the solver based on the PFFT library.

2.3 Fast multipole method (FMM)

The fast multipole method was first proposed in 1987 for 2D systems,[43] and it was soon extended to 3D problems.[44] Although only $\mathcal{O}(N)$ operations are necessary to calculate the electrostatic potential, the first FMM versions had big prefactors that in practice made the method competitive only for huge systems or low accuracy calculations.[45] After thorough research, it was possible to develop signficantly more accurate and efficient versions of FMM,[46,47] making it a largely celebrated method.[48]

The original FMM was devised to calculate the potential generated by a set of discrete point-like particles, this is

$$v(\boldsymbol{r}_i) = \frac{1}{4\pi\varepsilon_0} \sum_{j=1, j\neq i}^{N} \frac{q_j}{\left|\boldsymbol{r}_i - \boldsymbol{r}_j\right|} \,, \tag{13}$$

which is different from the charge-distribution problem that we are studying in this work. While extensions of FMM to the continuous problem exist,[49–51] in order to profit from the efficient parallel FMM implementations we have devised a simple scheme to recast the continuous problem into a discrete charge one without losing precision.

We assume that each grid point $r_{j,k,l}$ corresponds to a charge of magnitude $\Omega\rho_{j,k,l}$, where $\Omega = L^3$ (L being the grid spacing) is the volume of the space associated to each grid point (cell volume). Using FMM we calculate at each point the potential generated by this set of charges, $v^{\mathrm{FMM}}_{j,k,l}$. However, this is not equivalent to the potential generated by the charge distribution, and some correction terms need to be included (see supporting info[52] for the derivation of these corrections). The first correcting term (self-interaction term) comes from the potential generated at

each point by the charge contained in the same cell

$$v^{\mathrm{SI}}_{j,k,l} = 2\pi \left(\frac{3}{4\pi}\right)^{2/3} L^2 \rho_{j,k,l} \ . \tag{14}$$

Additionally, we apply a correction to improve the accuracy of the interaction between neighbouring points, which has the largest error in the point-charge approximation. This correction term is derived using a formal cubic interpolation of the density to a finer grid, obtaining a simple finite-differences-like term

$$\begin{aligned} v^{\mathrm{corr.}}_{j,k,l} &= L^2\big(27/32 + (\alpha)2\pi(3/4\pi)^{2/3}\big)\rho_{j,k,l} \\ &+ (L^2/16)\big(\rho_{j-1,k,l} + \rho_{j+1,k,l} + \rho_{j,k-1,l} + \rho_{j,k+1,l} + \rho_{j,k,l-1} + \rho_{j,k,l+1}\big) \\ &- (L^2/64)\big(\rho_{j-2,k,l} + \rho_{j+2,k,l} + \rho_{j,k-2,l} + \rho_{j,k+2,l} + \rho_{j,k,l-2} + \rho_{j,k,l+2}\big) \ . \end{aligned} \tag{15}$$

Here α is a parameter to compensate the charge within the cell (j,k,l) that is counted twice. The final expression for the potential is

$$v_{j,k,l} = v^{\mathrm{FMM}}_{j,k,l} + v^{\mathrm{SI}}_{j,k,l} + v^{\mathrm{corr.}}_{j,k,l} \ . \tag{16}$$

Now we give a brief introduction of the FMM algorithm. More detailed explanations on FMM can be found in Refs.[43,44,46,53] The concrete implementation we used in this work is explained in.[47,54] To introduce the method we use spherical coordinates in what remains of this section.

Consider a system of l charges $\{q_i,\ i = 1,\ldots,l\}$ located at points $\{(\tau_i,\alpha_i,\beta_i),\ i = 1,\ldots,l\}$ which lie in a sphere D of radius a and center at $Q = (\tau,\alpha,\beta)$. It can be proved[46] that the electric field created by them at a point $P = (r,\theta,\phi)$ outside D is

$$v(P) = \sum_{n=0}^{\infty} \sum_{m=-n}^{n} \frac{O_n^m}{(r')^{n+1}} Y_n^m(\theta',\phi') \ , \tag{17}$$

where $P-Q=(r',\theta',\phi')$ and

$$O_n^m=\sum_{i=1}^{l} q_i \tau_i^n Y_n^{-m}(\alpha_i,\beta_i)\ , \tag{18}$$

with $Y_n^m(\alpha,\beta)$ known functions (the spherical harmonics). If P lies outside of a sphere D_1 of radius $a+\tau$ (see Figure 2 A) the potential of Eq. (17) can be re-expressed as

$$v(P)=\sum_{j=0}^{\infty}\sum_{k=-j}^{j}\frac{M_j^k}{r^{j+1}}Y_j^k(\theta,\phi)\ , \tag{19}$$

where

$$M_j^k=\sum_{n=0}^{j}\sum_{m=-n}^{n}\frac{O_{j-n}^{k-m}\ i^{|k|-|m|-|k-m|}\sqrt{(j-n-k+m)!(j-n+k-m)!}\sqrt{(n-m)!(n+m)!}\ \tau^n\ Y_n^{-m}(\alpha,\beta)}{\sqrt{(j-k)!(j+k)!}}\ . \tag{20}$$

Note that the "entangled" expression of the potential equation Eq. (13), in which the coordinates of the point where the potential is measured and the coordinates of the charge that creates the potential are together, has been converted to a "factorised" expression, in which the coordinates of the point where we measure the potential are in terms $(Y_j^k(\theta,\phi)/r^{j+1})$ that multiply terms (M_j^k) which depend on the coordinates of the charges that create the potential. It is this factorisation which enables efficient calculation of the potential that a set of charges creates at a given point by using the (previously calculated) expression of the potential created by this set of charges at other points.

If the set of l charges described above is located inside a sphere D_Q of radius a with center at $Q=(\tau,\alpha,\beta)$ where $\tau>2a$ (see Figure 2 B) then equation Eq. (17) implies that the potential created by these charges inside a sphere D_0 of radius a centered at the origin is given by

$$v(P)=\sum_{j=0}^{\infty}\sum_{k=-j}^{j} L_j^k\ r^j\ Y_j^k(\theta,\phi)\ , \tag{21}$$

where

$$L_j^k = \sum_{n=0}^{\infty} \sum_{m=-n}^{n} \frac{O_n^m \, i^{|k-m|-|k|-|m|} \sqrt{(n-m)!(n+m)!} \sqrt{(j-k)!(j+k)!} \, Y_{j+n}^{m-k}(\alpha,\beta)}{(-1)^n \, \tau^{j+n+1} \, \sqrt{(j+n-m+k)!(j+n+m-k)!}} \, . \tag{22}$$

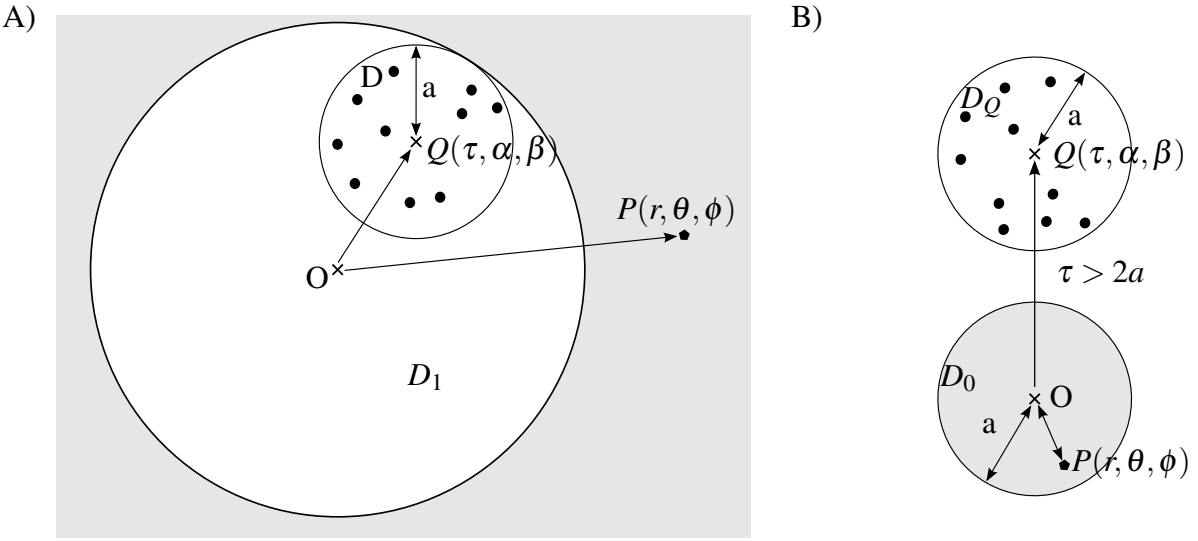

Figure 2: A) A set of point charges (black circles) inside a sphere D of radius a centred at $Q = (\tau,\alpha,\beta)$ creates a potential outside the sphere D_1 of radius $(a+\tau)$ and centred in the origin that can be expressed with equation Eq. (19). B) A set of point charges (black circles) inside a sphere D_Q of radius a centred at $Q = (\tau,\alpha,\beta)$ creates a potential inside the sphere D_0 of radius a and centred in the origin that can be expressed with equation Eq. (21) (provided that $\tau > 2a$). In both A) and B), O represents the origin of coordinates, and $P = (r,\theta,\phi)$ is the point where the potential is measured. In our systems, the charges lie in equispaced grid points.

The evaluation of the equations above requires truncation of the infinite sums to a given order, which can be chosen to keep the error below a given threshold. The equations Eq. (19) and Eq. (21) enable the efficient calculation of the potential experienced by every charge of the system due to the influence of the other charges. In order to calculate it, the system is divided into a hierarchy of boxes. Level 0 is a single box containing the whole system; level 1 is a set of 8 boxes containing level 0; and so on (a box of level $\mathscr{L}$ consists of 8 boxes of level $\mathscr{L}+1$). Different boxes at a given level do not contain common charges. The highest level ($\mathscr{N}_l$) contains several charges (in our case, each lying in a grid point) in every box. The procedure to calculate the potential in all grid points can be summarised as follows:

- For every box in the highest box level $\mathscr{N}_l$ (smallest boxes), we calculate the potential created

by the charges in that box using equation Eq. (17).

- We gather 8 boxes of level $\mathscr{N}_l$ to form every box of level $\mathscr{N}_l$-1. We calculate the potential created by the charges of the $(\mathscr{N}_l - 1)$-box using the potentials created by the eight $(\mathscr{N}_l)$-boxes that form it. To this end, we use equation Eq. (19).

- We repeat this procedure (we use equation Eq. (19) to get the potentials created by box $\mathscr{L}$-1 by using those of box $\mathscr{L}$) until all the levels are swept.

- Then, the box hierarchy is swept in the opposite direction: from lower to higher levels, the equation Eq. (21) is used to calculate the potential created by the boxes (the potential given by equation Eq. (21) is valid in regions that are not equal to those where equation Eq. (19) is valid).

- Finally, the total potential in every grid point ($v^{FMM}_{j,k,l}$) is calculated as an addition of three terms: the potentials due to nearby charges are directly calculated with the pairwise formula equation Eq. (13), and the potentials due to the rest of the charges are calculated either with equation Eq. (19) or with equation Eq. (21), depending on the relative position of the boxes which create the potential and the box where the potential is evaluated.

In the whole procedure above, the charge in the grid point (j,k,l) is $\Omega\rho_{j,k,l}$. This scheme corresponds to the traditional version of FMM.[46] We used a slight modification of it[54] which not only converts multipoles between consecutive levels, but also within every given level, which enables further computational savings.

2.4 Conjugate gradients

We now present two widely used iterative methods to calculate the electrostatic interaction: conjugate gradients and multigrid.[55] These methods are based on finding a solution to the Poisson equation Eq. (2) by starting from an initial guess and systematically refining it so that it becomes

arbitrarily closer to the exact solution. These two methods have the advantage that if a good initial approximation is known, only a few iterations are required.

When using a grid representation, the Poisson equation can be discretised using finite differences. In this scheme the Laplacian at each grid point is approximated by a sum over the values of neighbouring points multiplied by certain weights. High-order expressions that include several neighbours can be used to control the error in the approximation.[56] The finite-difference approximation turns equation (Eq. (2)) into a linear algebraic equation

$$\tilde{L}\boldsymbol{x} = \boldsymbol{y} \,, \tag{23}$$

where $\tilde{L}$ is a sparse matrix (taking advantage of the sparsity of a system of equations can greatly reduce the numerical complexity of its solution[57]), $\boldsymbol{y}$ is known ($y = -\rho/\varepsilon_0$, in this case) and $\boldsymbol{x}$ is the quantity we are solving for, in this case the electrostatic potential. Equation (Eq. (23)) can be efficiently solved by iterative methods that are based on the application of the matrix-vector product without the need to store the matrix.

Since the matrix is symmetric and positive definite, we can use the standard conjugate gradients[58] (CG) method. CG builds $\boldsymbol{x}$ as a linear combination of a set of orthogonal vectors $\boldsymbol{p}_k$. In every iteration, a new term is added

$$\boldsymbol{x}_{k+1} = \boldsymbol{x}_k + \alpha_{k+1}\boldsymbol{p}_{k+1} \,, \tag{24}$$

which attempts to minimise

$$f(\boldsymbol{x}) := \frac{1}{2}\boldsymbol{x}^T\tilde{L}\boldsymbol{x} - \boldsymbol{x}^T\boldsymbol{y} \,, \tag{25}$$

whose minimum is the solution of equation Eq. (23). The term added to the potential in iteration k is built so that $\boldsymbol{x}$ moves in the direction of the gradient of f but being orthogonal to the previous terms. The gradient of $f(\boldsymbol{x})$ satisfies, $-\nabla f(\boldsymbol{x}) = \boldsymbol{y} - \tilde{L}\boldsymbol{x}$. Therefore the search direction in iteration

$k+1$ is

$$\boldsymbol{p}_{k+1} = \left(\boldsymbol{y} - \tilde{L}\boldsymbol{x}_k\right) - \sum_{i \leq k} \frac{\boldsymbol{p}_i^T \tilde{L}(\boldsymbol{y} - \tilde{L}\boldsymbol{x}_k)}{\boldsymbol{p}_i^T \tilde{L}\boldsymbol{p}_i} \boldsymbol{p}_i \ . \tag{26}$$

The coefficient associated with each direction, α_{k+1}, is obtained from the minimization condition, yielding

$$\alpha_{k+1} = \left(\frac{\boldsymbol{p}_{k+1}^T (\boldsymbol{y} - \tilde{L}\boldsymbol{x}_k)}{\boldsymbol{p}_{k+1}^T \tilde{L}\boldsymbol{p}_{k+1}} \right) \ . \tag{27}$$

The equations above show that the conjugate gradients method has a linear scaling ($\mathscr{O}(N)$) with the number of points N for a given number of iterations whenever the matrix $\tilde{L}$ has a number of non-zero entries per row that is much lower than N (as is the usual case for the Poisson equation). Bigger exponents in the scaling can appear, however, in problems where the number of performed iterations is chosen to keep the solution error below a given threshold that depends on N.[59]

The parallelisation of our CG implementation is based on the domain decomposition approach, where the grid is divided into subregions that are assigned to each process. Since the application of the finite-difference Laplacian only requires near-neighbour values, only the boundary values need to be shared between processors (see refs.[14,60] for details). Since our implementation can work with arbitrary shape grids, dividing the grids into subdomains of equal volume while minimizing the area of the boundaries is not a trivial problem, for this task we use the Metis library.[61]

An issue that appears when using the finite-difference discretisation to solve the Poisson equation are boundary conditions: they must be given by setting the values of the points on the border of the domain. For free space boundary conditions we need a secondary method to obtain the value of the potential over these points; this additional method can represent a significant fraction of the computational cost and can introduce an approximation error. In our implementation we use a multipole expansion.[62]

2.5 Multigrid

Multigrid[55,63–67] is a powerful method to solve elliptic partial differential equations, such as the Poisson problem,[68] in an iterative fashion. Multigrid is routinely used as a solver or precondi-

tioner for electronic structure and other scientific applications.[69–72] In this section we will make a brief introduction to a simple version of the multigrid approach that is adequate for the Poisson problem. Multigrid, however, can also be generalized to more complex problems, like non-linear problems[67] and systems where there is no direct geometric interpretation, in what is known as algebraic multigrid.[73] It has also been extended to solve eigenvalue problems.[71,74]

Multigrid is based on iterative solvers like Jacobi or Gauss-Seidel.[55] These methods are based on a simple iteration formula, that for equation Eq. (23) reads

$$\boldsymbol{x} \leftarrow \boldsymbol{x} + M^{-1}(\boldsymbol{y} - \tilde{L}\boldsymbol{x}) \; . \tag{28}$$

The matrix M is an approximation to $\tilde{L}$ that is simple to invert. In the case of Jacobi, M is the diagonal of $\tilde{L}$, and for Gauss-Seidel, M is upper diagonal part of $\tilde{L}$. These methods are simple to implement, in particular in the case of the Laplacian operator, but are quite inefficient by themselves, so they are not practical as linear solvers for high-performance applications. However, they have a particular property: they are very good in removing the high-frequency error of a solution approximation, where the frequency is defined in relation to the grid spacing. In other words, given an approximation to the solution, a few iterations of Jacobi or Gauss-Seidel will make the solution smooth. In multigrid the smothing property is exploited by using a hierarchy of grids of different spacing, and hence changing the frequency that these smoothing operators can remove efficiently.

A fundamental concept in multigrid is the residual of a linear equation. If we have $\bar{x}$ as an approximate solution of equation Eq. (23), the associated residual, $\boldsymbol{b}$, is defined as

$$\boldsymbol{b} = \boldsymbol{y} - \tilde{L}\bar{\boldsymbol{x}} \; . \tag{29}$$

We can use the residual to define an alternative linear problem

$$\tilde{L}\boldsymbol{a} = \boldsymbol{b} \; . \tag{30}$$

Due to the linearity of the Laplacian operator, finding $\boldsymbol{a}$ is equivalent to solving the original linear problem, equation Eq. (23), as

$$\boldsymbol{x} = \bar{\boldsymbol{x}} + \boldsymbol{a}. \tag{31}$$

If a few iterations of a smoothing operator have been applied to the approximate solution, $\bar{x}$, we know that the high-frequency components of the corresponding residual $\boldsymbol{b}$ should be small. Then it is possible to represent $\boldsymbol{b}$ in a grid that has, for example, two times the spacing without too much loss of accuracy. In this coarser grid equation Eq. (30) can be solved with less computational cost. Once the solution $\boldsymbol{a}$ is found on the coarser grid, it can be transferred back to the original grid and used to improve the approximation to the solution using equation Eq. (31).

The concept of calculating a correction term in a coarser grid is the basis of the multigrid approach. Instead of two grids, as in our previous example, a hierarchy of grids is used, at each level the residual is transferred to a coarser grid where the correction term is calculated. This is done up to the coarsest level that only contains a few points. Then the correction is calculated and transferred back to the finer levels.

To properly define the multigrid algorithm it is necessary to specify the operators that transfer functions between grids of different spacing. For transferring to a finer grid, typically a linear interpolation is used. For transferring to a coarser grid a so-called restriction operator is used. In a restriction operator, the value of the coarse grid point is calculated as a weighted average of the values of the corresponding points in the fine grid and its neighbors.

Now we introduce the multigrid algorithm in detail. Each quantity is labeled by a super-index that identifies the associated grid level, with 0 being the coarsest grid and L the finest. We denote S^l as the smoothing operator at level l, which corresponds to a few steps (usually 2 or 3) of Gauss-Seidel or Jacobi. I_l^m represents the transference of a function from the level l to the level m by restriction or interpolation. Following these conventions, we introduce the algorithm of a multigrid iteration in fig. Figure 3. Given an initial approximation for the solution, we perform a few steps of the smoothing operator, after which the residual is calculated and transferred to the coarser grid. This iteration is repeated until the coarsest level is reached. Then we start to move towards finer

grids. In each step the approximate solution of each level is interpolated into the finer grid and added, as a correction term, to the solution approximation of that level, after which a few steps of smoothing are performed. Finally, when the finest level is reached, a correction term that has contributions from the whole grid hierarchy is added to the initial approximation to the solution.

Multigrid *v*-cycle
Input: $\boldsymbol{y}, \bar{\boldsymbol{x}}$
Output: $\bar{\boldsymbol{x}}$

$\boldsymbol{y}^L \leftarrow \boldsymbol{y}$
$\boldsymbol{x}^L \leftarrow \bar{\boldsymbol{x}}$
for l from L to 0 **do**
  if $l \neq L$ **then**
    $x^l \leftarrow 0$ {Set initial guess to 0}
  end if
  $\boldsymbol{x}^l \leftarrow \mathrm{S}^l \boldsymbol{x}^l$ {Pre-smoothing}
  if $l \neq 0$ **then**
    $\boldsymbol{b}^l \leftarrow \boldsymbol{y}^l - \tilde{L}^l \boldsymbol{x}^l$ {Calculate the residual}
    $\boldsymbol{y}^{l-1} \leftarrow I_l^{l-1} \boldsymbol{b}^l$ {Transfer the residual to the coarser grid}
  end if
end for
for l from 0 to L **do**
  if $l \neq 0$ **then**
    $\boldsymbol{x}^l \leftarrow \boldsymbol{x}^l + I_{l-1}^l \boldsymbol{x}^{l-1}$ {Transfer the correction to the finer grid}
  end if
  $\boldsymbol{x}^l \leftarrow \mathrm{S}^l \boldsymbol{x}^l$ {Post-smoothing}
end for
$\bar{\boldsymbol{x}} \leftarrow \boldsymbol{x}^L$

Figure 3: Algorithm of a multigrid *v*-cycle.

The scheme presented in Figure 3 is known as a *v*-cycle, for the order in which levels are visited, some more sophisticated strategies exist, where the coarsest level is visited twice (a *w*-cycle) or more times before coming back to the finest level.[67] Usually a *v*-cycle reduces the error, measured as the norm of the residual, by around one order of magnitude, so typically several *v*-cycles are required to find a converged solution.

When a good initial approximation is not known, an approach known as full multigrid (FMG) can be used. In FMG the original problem is solved first in the coarsest grid, then the solution is interpolated to the next grid in the hierarchy, where it is used as initial guess. The process is

repeated until the finest grid is reached. It has been shown that the cost of solving the Poisson equation by FMG depends linearly with the number of grid points.[67]

Just as in the case of conjugate gradients, the parallelisation of multigrid is based on the domain decomposition approach. However in the case of multigrid some additional complications appear. First of all, as coarser grids are used the domain decomposition approach becomes less efficient as the number of points per domain is reduced. Secondly, the Gauss-Seidel procedure used for smoothing should be applied to each point sequentially[67] so it is not suitable for domain decomposition. In our implementation we take the simple approach of applying Gauss-Seidel in parallel over each domain. For a large number of domains, this scheme would in fact converge to the less-efficient Jacobi approach.

3 Methods

3.1 Implementation

We chose the OCTOPUS code[14,60,75] (revision 8844) [a] for our tests on the features of Poisson solvers in the context of quantum mechanics. OCTOPUS is a program for quantum *ab initio* simulations based on density functional theory and time-dependent density functional theory for molecules, one-dimensional systems, surfaces, and solids under the presence of arbitrary external static and time-dependent fields. Its variables are represented on grids in real space[b] (not using a basis of given functions), which feature allows for systematic control of the discretisation error, of particular importance for excited-state properties.[77] Furthermore, OCTOPUS uses a multi-level parallelisation scheme where the data is distributed following a tree-based approach. This scheme uses the message passing interface (MPI) library and was shown to be quite efficient in modern parallel computers.[14] We incorporated recent massively parallelisable versions of the fast Fourier transform[33] and of the fast multipole method[47] into OCTOPUS. The goal of our tests was to measure

[a] The OCTOPUS code is available in a public Subversion repository `http://www.tddft.org/svn/octopus/trunk`.

[b] Real space codes are at present a popular option; see e.g.[76]

execution-times and accuracies of the six selected Poisson solvers, as a function of the system size and the number of parallel processes. Highlights in our implementation are a novel correcting term to adapt the FMM method to charge distributions, and a smart, fast way to manage the data flow for the PFFT.

One must take into account that the execution-time of a function (like a Poisson solver) included in a bigger program (in this case OCTOPUS) is determined not only by the function itself, but also by some features of the main program, like the way it represents the data and the pattern for the data flow between the function and the main program. An example of this is the case when the FFT method (or ISF, which is based on FFT's) are used in a code where the spatial functions are represented in a Cartesian grid of arbitrary shape (like OCTOPUS). Fast Fourier transforms require parallelepiped grids, while the shape for the grid used in OCTOPUS is commonly rather amorphous to reduce the total number of points. So, whenever OCTOPUS evaluates a fast Fourier transform, a parallelepiped mesh containing the original amorphous mesh is used, and the new entries are filled with zeroes. The library PFFT divides such a parallelepiped grid using a 2D grid of processes (see section Section 2.1) as displayed in Figure 4 B. This means that each process must handle the data corresponding to a column-like dataset (i.e., a dataset that includes all the range of points in a given direction direction; for example $\rho_{j,k,l}$ with $j = 1,\ldots,n_1/4$, $k = n_2/4+1,\ldots,2n_2/4$ and $l = 1,\ldots,n_3$, where $N = n_1 n_2 n_3$). On the other hand, OCTOPUS divides the space grid into more compact domains, each handled by a process (see Figure 4 A), to reduce the surface separating domains and consequently to reduce the need for information transfer between processes. Therefore, the data that a process deals with in the OCTOPUS main program is not the same as the PFFT library uses inside, and hence a data transfer is necessary.

The simplest way to carry this data-transfer out is to gather all the data (density ρ or potential v) in all the processes before copying them from one grid to the other. Unfortunately, this solution does not scale well to a large number of processors and cannot be used in massively parallel applications. Nevertheless, we have to use this technique with the serial FFT, because of its serial nature, and with ISF solvers, because the kernel of the ISF solver needs to work with entire vectors

in all processes.

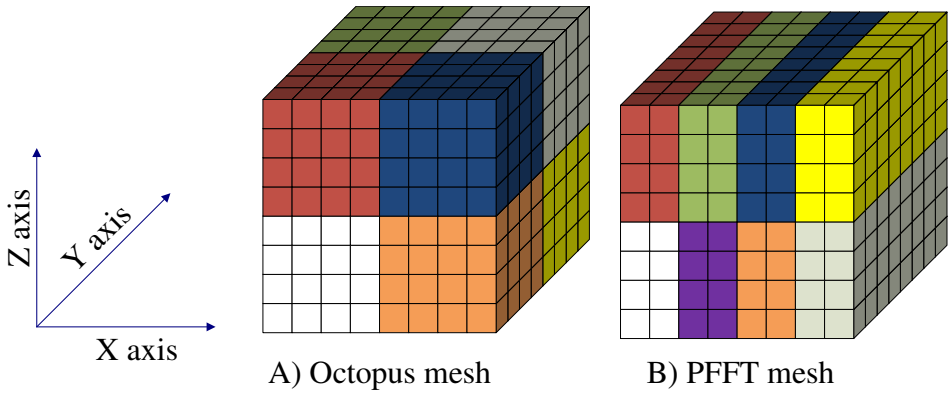

Figure 4: Simplified domain decomposition of the simulation meshes. Each little cube represents a grid point (8^3 points in total) and each colour represents a partition (8 partitions). A) OCTOPUS mesh with a 3D domain decomposition; B) PFFT mesh with a 2D decomposition.

This problem is overcome as follows in the PFFT-based method as implemented in OCTOPUS. At the initialization stage of OCTOPUS, a mapping between the OCTOPUS mesh decomposition and the PFFT mesh decomposition is established and saved. This mapping is used when running the actual solver to efficiently communicate only the strictly necessary grid data, achieving almost perfectly linear parallel scaling. In addition, all the data-structures of the Poisson solver (mainly density ρ or potential v) are partitioned among all the processes. In this manner, memory requirement per core decreases when more processors are available, and hence, bigger physical systems can be simulated.

The correction for the FMM method (see section Section 2.3) was also implemented in a very efficient way, re-expressing its formula for each point to avoid accessing the same memory position (which stores the charge density of a neighbour of the point where the correction is being calculated) more than once. Further details about the data-transfer implementation and the correction method applied to FMM can be found in the supporting info.

3.2 Test on high-performance supercomputing facilities

For carrying our tests out, we have used some of the most powerful computational resources existing at present in Europe: Curie in France —at Commissariat à l'Energie Atomique (CEA)— and

two IBM Blue Gene/P machines —Jugene at the Jülich Supercomputing Center, and Genius at the Rechenzentrum Garching of the Max Planck Society—. In addition, we have run some tests in a smaller cluster (Corvo), to provide contrast in the lower range of the number of processors. All four machines are considered to be representative of the current trends of scientific High Performance Computing.[78–80]

The IBM Blue Gene/P systems are based on PowerPC 450 chips at 850 MHz. One chip consists of 4 cores, and it is soldered to a small motherboard, together with memory (DRAM), to create a compute card (one node). The amount of RAM per compute card is 2 GiB and they do not have any type of hard disk. Two rows of 16 compute cards each are plugged into one board to form a node card. A rack holds a total of 32 node cards, and in total there are 72 racks (294,912 cores) in Jülich Blue Gene/P (Jugene), and 4 racks (16,384 cores) in Garching (Genius). Each computing node of Blue Gene/P has 4 communication networks: (a) a 3D torus network for point-to-point communication, 2 connections per dimension; (b) a network for collective communications; (c) a network for barriers; and (d) a network for control. I/O nodes, in addition, are connected to a 10 gigabit Ethernet network.

On the other hand, the Curie supercomputer is based on Intel Xeon X7560 processors at 2.6 GHz. Each compute node, called "fat node", has 32 cores (4 chips of 8 cores each) and 128 GiB of RAM. The compute nodes are connected with an Infiniband network. In total 11,520 cores and almost 46 TB of RAM are available.

Finally, the configuration of the cluster Corvo, of the Spanish node of the ETSF and Nano-Bio Spectroscopy group, is similar to the Curie supercomputer, although in a lower scale. Both the manufacturer (Bull SAS) and the architecture (x86-64) are the same. More specifically, each node of Corvo has two Intel Xeon E5645 of 6 cores and 48 GiB of RAM. There are 960 cores in total, connected with QDR Infiniband.

4 Results

In this section we present the results of our tests to measure the execution time and accuracy of the Poisson solvers discussed in section Section 2. We estimate their quality in terms of speed-up and accuracy, as well as make some remarks on the influence of some input parameters on them. More tests and scalability comparisons are presented in the supporting info accompanying this paper.

4.1 Accuracy

We calculate the Hartree potential created by Gaussian charge distributions in an important part of our tests. Such a potential can be calculated analytically, and hence the error made by any method can be measured by comparing the two results: numerical and analytical. We defined two different variables to measure the accuracy of a Poisson solver, D and F, as follows:

$$D := \frac{\sum_{ijk} |v_a(\boldsymbol{r}_{ijk}) - v_n(\boldsymbol{r}_{ijk})|}{\sum_{ijk} |v_a(\boldsymbol{r}_{ijk})|} \,, \tag{32a}$$

$$E_a = \frac{1}{2} \sum_{ijk} \rho(\boldsymbol{r}_{ijk}) v_a(\boldsymbol{r}_{ijk}) \,, \tag{32b}$$

$$E_n = \frac{1}{2} \sum_{ijk} \rho(\boldsymbol{r}_{ijk}) v_n(\boldsymbol{r}_{ijk}) \,, \tag{32c}$$

$$F := \frac{E_a - E_n}{E_a} \,, \tag{32d}$$

where $\boldsymbol{r}_{ijk}$ are all the points of the analysed grid, v_a is the analytically calculated potential, and v_n is the potential calculated by either the PFFT, ISF, FMM, CG, or multigrid-based method. E_a and E_n are the expressions for the Hartree energies obtained using the potentials that were calculated analytically and numerically, respectively. These variables provide an estimate of the deviations of the calculated potential and energy from their exact values. D gives a comprehensive estimate of the error, for it takes into account the calculated potential in all points. The total Hartree energy coming from these potentials is a physically relevant variable, so an estimate of its error is also meaningful.

In Table 1 we display some values of D and F for the tested Poisson solvers. The input charge distributions correspond to Gaussian distributions represented in cubic grids with variable edge ($2L_e$) and constant spacing between consecutive points ($L = 0.2$ Å). The additional OCTOPUS parameters we use are: `PoissonSolverMaxMultipole = 7` (for multigrid and conjugate gradients), `MultigridLevels = max_levels` (i.e. use all available multigrid levels in the multigrid calculation), `DeltaEFMM = 0.0001` and `AlphaFMM = 0.291262136` (for the fast multipole method). Further information on these parameters can be found in section Section 4.3 and in the supplementary material. From Table 1 it can be said that FFT-based methods

Table 1: F and D errors of different Poisson solvers in the calculation of the Hartree potential created by a Gaussian charge distribution represented on a grid of edge $L_e = 15.8$ Å and spacing 0.2 Å.

F error:

L_e (Å)	PFFT	ISF	FMM	CG	Multigrid
7	$2{\cdot}10^{-3}$	$2{\cdot}10^{-3}$	$2{\cdot}10^{-3}$	$2{\cdot}10^{-3}$	$2{\cdot}10^{-3}$
10	$9{\cdot}10^{-6}$	$9{\cdot}10^{-6}$	$4{\cdot}10^{-6}$	$4{\cdot}10^{-6}$	$9{\cdot}10^{-6}$
15.8	$2{\cdot}10^{-12}$	$3{\cdot}10^{-7}$	$3{\cdot}10^{-6}$	$3{\cdot}10^{-5}$	$5{\cdot}10^{-6}$
22.1	$<2{\cdot}10^{-12}$	$1{\cdot}10^{-11}$	$3{\cdot}10^{-6}$	$4{\cdot}10^{-4}$	$-1{\cdot}10^{-6}$
25.9	$<2{\cdot}10^{-12}$	$9{\cdot}10^{-12}$	$-4{\cdot}10^{-6}$	$5{\cdot}10^{-3}$	$2{\cdot}10^{-7}$
31.7	$<4{\cdot}10^{-13}$	$8{\cdot}10^{-12}$	$-3{\cdot}10^{-6}$	$1{\cdot}10^{-2}$	$-5{\cdot}10^{-7}$

D error:

L_e (Å)	PFFT	ISF	FMM	CG	Multigrid
7	$9{\cdot}10^{-3}$	$4{\cdot}10^{-3}$	$4{\cdot}10^{-3}$	$4{\cdot}10^{-3}$	$4{\cdot}10^{-3}$
10	$1{\cdot}10^{-4}$	$2{\cdot}10^{-5}$	$8{\cdot}10^{-5}$	$3{\cdot}10^{-5}$	$2{\cdot}10^{-5}$
15.8	$6{\cdot}10^{-5}$	$2{\cdot}10^{-7}$	$1{\cdot}10^{-4}$	$5{\cdot}10^{-5}$	$6{\cdot}10^{-6}$
22.1	$1{\cdot}10^{-5}$	$4{\cdot}10^{-10}$	$3{\cdot}10^{-4}$	$3{\cdot}10^{-4}$	$2{\cdot}10^{-6}$
25.9	$4{\cdot}10^{-7}$	$7{\cdot}10^{-10}$	$3{\cdot}10^{-4}$	$5{\cdot}10^{-3}$	$4{\cdot}10^{-7}$
31.7	$4{\cdot}10^{-8}$	$1\cdot10^{-9}$	$2{\cdot}10^{-4}$	$1{\cdot}10^{-2}$	$4{\cdot}10^{-7}$

(ISF, PFFT and FFT serial) give the best accuracies. Moreover, the multigrid and conjugate gradient solvers do not produce appropriate results when the set of grid points corresponds to an adapted shape (as is the usual case in OCTOPUS), and must be used with compact shapes (such as spherical or parallelepiped). Conjugate gradient methods' accuracy is acceptable for this type of test. Nevertheless, they show some problems if used in the calculation of the ground state of a set of electrons to solve the Kohn-Sham equation or to perform time-dependent density functional theory

calculations (which require calculation of the Hartree potential). The iterative procedure inherent to the used conjugate gradient method sometimes shows some convergence problems.

Other than using D and F (which depend solely on the charge density and Hartree potential), another way to measure accuracy is to calculate the ground state of a given system and check the effect of the Poisson solver on some of its corresponding quantities. We calculated the ground state of a system of chlorophyll stretches containing 180 atoms[81] (see supporting info for atomic system information). To this end, we used pseudopotentials, so 460 electrons appeared in the calculation. The grid shape was a set of spheres of radius 4.0 Å centred at the nuclei, and the grid spacing was 0.23 Å. The exchange correlation functional was the LDA functional.[82] In Table 2 we display the value of the Hartree energy, the highest eigenvalue, and the HOMO-LUMO gap. PFFT is expected to provide the most accurate results (by considering Table 1). However, the differences among all five methods can be considered negligible (lower than the errors introduced by the density functional theory exchange-correlation functional). The maximum difference of Hartree energy divided by the number of electrons is less than 0.015 eV. The maximum difference in the HOMO-LUMO gap is less than 0.0092 eV.

Table 2: Comparison of some quantities corresponding to the ground state of a set of chlorophyll stretches with 180 atoms.

	Hartree energy (eV)	HOMO (eV)	HOMO-LUMO gap (eV)
PFFT	240820.70	-4.8922	1.4471
ISF	240821.48	-4.8935	1.4489
FMM	240817.29	-4.8906	1.4429
CG	240815.01	-4.9009	1.4521
Multigrid	240814.69	-4.8979	1.4506

4.2 Execution time

In order to gauge the performance of the Poisson solvers, we have measured the total execution time that the calculation of the classical potential took for each method as a function of the number of processes involved in the resolution (regardless of initialisation times). We ran one single MPI

process per core on Curie and Corvo, and only one MPI process per node on Blue Gene/P's.[83] When possible, we ran the same set of standard tests on each of these machines. However, in cases where the size of the simulated system is high, the limited amount of memory per core becomes a serious problem. This problem is critical in Blue Gene/P machines, which have only 2 GiB per node, i.e. 512 MiB per core, so we executed one MPI process per node, with four OpenMP threads. The Curie supercomputer offers 4 GiB per core, but in some cases we could use more memory by selecting more cores and keeping them idle. Runs up to 4096 processes were only possible in Blue Gene/P and Curie machines; for Corvo it was only possible to run up to 512 MPI processes.

In our efficiency tests we calculated the potential created by Gaussian charge distributions represented in cubic grids with edge length $2L_e$, where L_e is half the edge of the parallelepiped mesh and the used values were 7.0, 10.0, 15.8, 22.1, 25.9 and 31.7 respectively (always with a spacing of 0.2). The smallest simulated system, with $L_e = 7$, contains $[2 * L_e/spacing + 1]^3 = 357,911$ grid points. By reason of memory limitations, the largest system simulated on a Blue Gene/P had $L_e = 25.9$ ($17,373,979$ points). On the Corvo and Curie machines, we were able to run a bigger system of $L_e = 31.7$ ($31,855,013$ points). For the FFT-based methods we used an additional box, ranging from 143^3 to 637^3 (up to 525^3 on a Blue Gene/P).

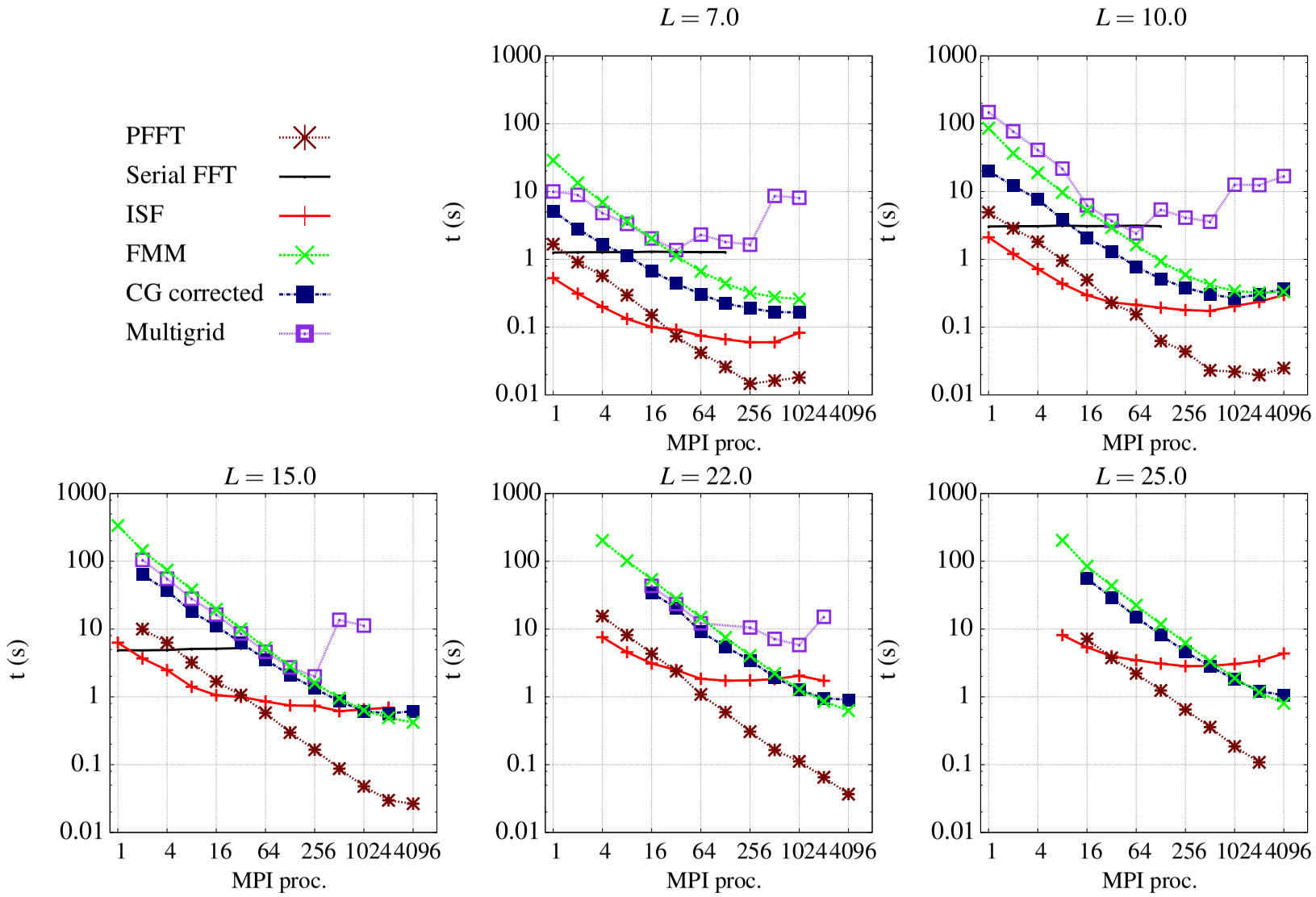

Figure 5: Execution times for the calculation of the Hartree potential created by a Gaussian charge distribution on a Blue Gene/P machine as a function of six different Poisson solvers and of the involved number of MPI processes (each MPI process having 4 OpenMP threads) for different simulated system sizes ($[2 * L_e/0.2 + 1]^3$ points).

First, we present the results obtained on a Blue Gene/P machine in Figure 5. Each graph of the figure represents a different problem size, with a different value of L_e. The X axis of Figure 5 shows the used number of MPI processes, each having 4 OpenMP threads. The Y axis is the time in seconds for the Poisson solver. Increasing memory requirements with higher L_e made some systems not able to fit in the available RAM memory, precluding the opportunity to run the serial FFT of size $L_e = 22.1$ and above, and multigrid of size $L_e = 25.9$ and above. One of the most memory consuming part of these tests was the generation of the mesh partitions, one per problem size per processor, regardless of the solver. Fortunately, these partitions must be done only once and they are machine independent. Moreover, they could be read from the restart files, which could also be transferred from one machine to another. However, this is not true of the multigrid solver, for which the mesh partition must be calculated for every multigrid level, which made it, impossible, for example, to run the system of size $L_e = 25.9$ due to the high memory requirement of the partitioning.

As can be observed in Figure 5, all the tests show a similar relative behaviour with regard to the system size under simulation and the number of MPI processes: execution times decrease with the number of processes until saturation, and larger systems allow the efficient use of a higher number of parallel processes, i.e., the solvers "saturates" at a higher number of processes. This is especially true for the newly implemented solvers, based on PFFT and FMM. Thus, this behaviour leaves the way open to simulate physical systems of more realistic size if tens of thousands of processors cores are available.

The multigrid solver shows the poorest results, and saturates with a relatively low number of parallel processes. The problem comes from the fact that only a limited number of multigrid levels can be used (obviously, every process needs to use at least one grid point to execute correctly). At most, we chose the closest natural number to $\log_8(N)$ as the number of multigrid levels, where N is the total number of grid points. In fact, if a high number of levels can be used, then the obtained speed-ups are appreciable, but execution times saturate, and even grow, when a few hundred of processors are used, so the number of multigrid levels in each process is then decreased.

Similarly, the ISF solver shows a limited efficiency; its nonlinear speed-up region appears at a relatively small number of processes. The main problem with the ISF solver is that the data-structures of OCTOPUS need to be transferred just before doing actual calculations and after finishing them. These global communication operations are done calling `MPI_Gatherv` and `MPI_Scatterv` functions, which do not scale linearly with the number of parallel processes.

The conjugate gradient and FMM methods seem to be very efficient approaches in terms of scalability. However, both become faster than ISF only when thousands of processes are used to simulate large physical systems, beyond 1024 parallel processes. The CG solver, too, has a limited accuracy and some convergence problems when it is used for solving the Poisson equation within TDDFT calculations in OCTOPUS.

Particularly attractive is the good performance obtained with the PFFT solver. Beginning at a low number of processes, execution times are always lower than those of the other solvers. In fact, 32 processes are enough to hide the overhead added by the parallelisation, and beyond this number of processes execution times become the best. This is because PFFT's communication patterns are so highly effective.

These tests have shown that the new implementations of the Poisson solvers, PFFT and FMM, offer good scalability and accuracy, and could be used efficiently when hundreds or thousands of parallel processes are needed. Almost linear performances can be observed until a saturation point is reached for all cases. There, the obtained efficiency factors[10] are always above 50% before those congestion points. As expected, large systems, which have higher computation needs, can make better use of a high number of processes.

A similar overall behaviour of the different solvers, with small differences, is also shown in the other two machines, Curie and Corvo. Figure 6 presents the obtained results for a particular case: $L_e = 15.8$. As can be observed, the best results are obtained again with the PFFT solver and a high number of parallel processes. Relative performance between the solvers varies slightly from the above analysed cases, but the conclusions are very similar.

For the serial case (only one processor), executions times are 4-5 times faster for Curie than

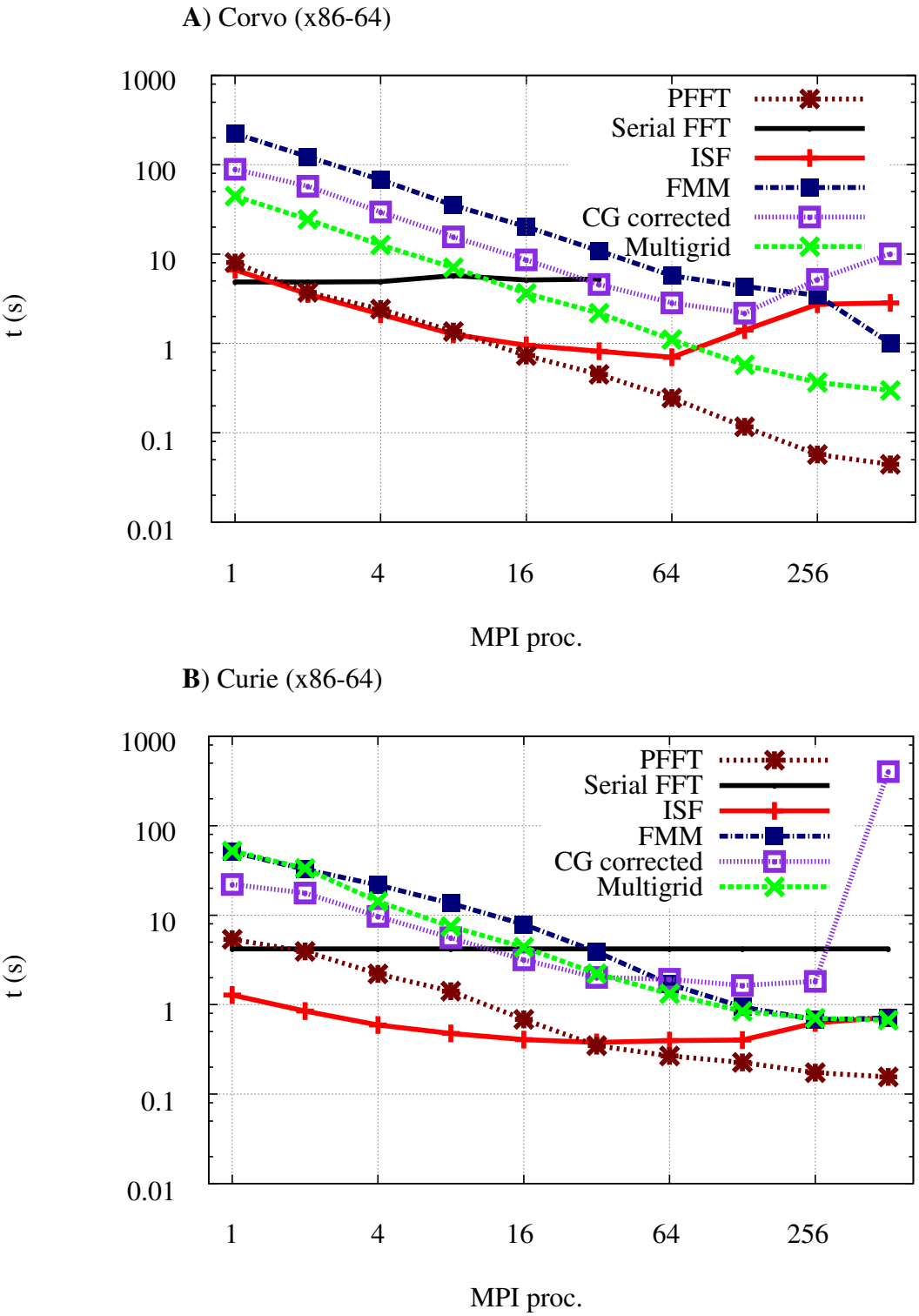

Figure 6: Execution times of the Poisson solver of size $L_e = 15.8$ in Corvo (A) and Curie (B) supercomputer for all the different solvers varying the number of MPI processes (each MPI process executed in a CPU processor core).

for Corvo, probably because of the size of the L3 cache, 24 MB in the processors of Curie (X7560 - Nehalem processors) and only 12 MB in Corvo (E5645 - Westmere processors). Similar performance has been reported for both processors using standard benchmarks [c], except for the case of dot products (vector code), where Curie's processor reaches 2.5 times more GFlop/s than Corvo's, which can also be understood as a consequence of the L3 cache differences.

At any rate, these differences tend to disappear when using a high number of processors, in part because the size of the problem assigned to each processor is smaller (and so the influence of the cache size is also lower), and in part because communication among processors, not only data processing, must also be considered.

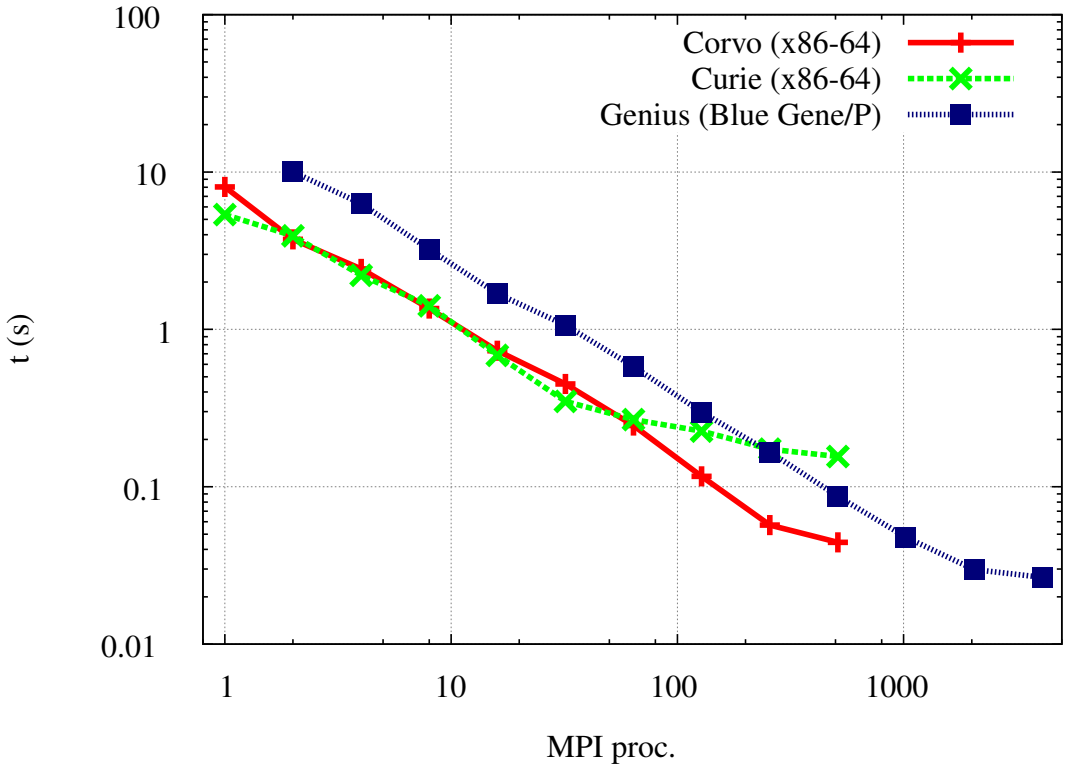

Figure 7: Execution times of the PFFT solver in Genius (Blue Gene/P), Curie and Corvo (x86-64) for a system size of $L_e = 15.8$ as a function of the number of MPI processes.

In order to compare more clearly the results obtained in the three computers, Figure 7 shows the execution times of the PFFT solver for the case of $L_e = 15.8$ in Blue Gene, Curie and Corvo.

[c] X7560: `http://browser.primatelabs.com/geekbench2/198947`
and E5645: `http://browser.primatelabs.com/geekbench2/389297`

Execution times are higher in the Blue Gene/P computers for the same number of processes, but scalability is much better, allowing the efficient use of a much higher number of processes. The processors of the Blue Gene/P machine are slower than those of Curie and Corvo, but communication infrastructures are much better (see section Section 3.2). This leads us to conclude that the execution time of the Poisson solver parallel code is closely related to the performance of the interprocessor communication system of the parallel computer, more so than on the performance of the processors themselves.

As stated in section Section 2, the numerical complexities of PFFT and FMM scale as $\mathscr{O}(N \log N)$ and $\mathscr{O}(N)$ respectively, with N the total number of points required. We have analysed the execution order by measuring the execution time on Blue Gene/Ps as a function of the volume of the system for PFFT and FMM in three cases: 16, 32 and 64 parallel processes. The volume ratio among the smallest ($L_e = 7$) and the largest ($L_e = 25.9$) studied systems is about 49. Our results agree with the $\mathscr{O}(N)$ complexity of the FMM method and the $\mathscr{O}(N \log N)$ complexity of the PFFT method. Note that computation time is appreciably higher when using the FMM solver due to its higher prefactor (the quantity that multiplies N or $N \log N$ in the expression of the numerical complexity). The quotient between prefactors is machine dependent; its value is about 5.5 for Corvo, about 9 for Curie and about 12 for Blue Gene/P. One may think that for very big values of N at a constant number of processes P, the growth of the term $\log N$ would eventually make FMM more efficient than PFFT. This is strictly true, but the huge N of this eventual crossover precludes it in practice. For example, our results using 16 cores indicate that this crossover would take place at $N > 10^{53}$ in Blue Gene/P, and at $N \simeq 4.5 \cdot 10^{41}$ in Corvo.

Apart from the speed-up and execution time of a concrete parallel execution, another very useful quality measure is the weak-scaling. Weak-scaling measures the ability of an algorithm to scale with the number of parallel processes at a fixed computing load, comparing the execution time of a problem of size N using P processes with the execution time of the same problem but of size kN using kP processes. In this way, each process will use the same amount of computational resources, regardless of the number of processors used. If the algorithm is mainly constricted by

computational needs, then execution times should be very similar in both cases. On the other hand, if communication needs dominates the parallel execution, then execution times will grow with P, usually faster than linearly. For these tests we have adapted the system sizes of the parallelepiped meshes to 7.9, 10, 15.8, 20.1 and 25.1 (also 31.7 in Corvo) for the Poisson solver on Blue Gene/P and Corvo. Since the number of grid points increases like the cube of L_e, we did parallel runs using 4, 8, 32, 64 and 128 MPI processes (256 processes in Corvo). So, the number of grid points processed in each parallel MPI process is roughly 125,000. Figure 8 shows the obtained results, with data taken from the profiling output.

On one hand, the weak-scaling factor of the ISF solver increases sharply with the number of parallel processes, certainly because of the communication needs of the method, and confirming the conclusions we have obtained previously. The conjugate gradient and multigrid methods show an important increase in the weak-scaling factor with the number of processes, and this can be used to predict that parallel execution will "saturate" at a moderate number of processes (as we had observed in Figure 5). In contrast, FMM shows the best results in the analysed range: weak-scaling increases very moderately, so we can conclude that communication overheads are quite acceptable and that the method will offer good speed-up results when using thousands of processes.

PFFT also gives very good results in the Blue Gene/P system. They are similar to those of FMM, so similar conclusions can be stated. Nonetheless, the results obtained in Corvo up to 256 processes seem to indicate that communication will play an important role if a high number of processes are to be used. In these cases, the efficiency of the communication network and protocols of the parallel computer will play an important role in the obtained parallel performance. This can already be observed in Figure 8: the weak-scaling factor is markedly better and bounded in Blue Gene/P, a system with a very high performance communication network. Also limited to the Corvo system, a sharp increment in the weak-scaling factor is observed when passing from 216 (within only one Infiniband switch, $12 \times 18 = 216$ cores) to 256 cores, that needs communication with processes in a second switch.

From all our tests, we conclude that the communication needs of the Poisson solvers fit better

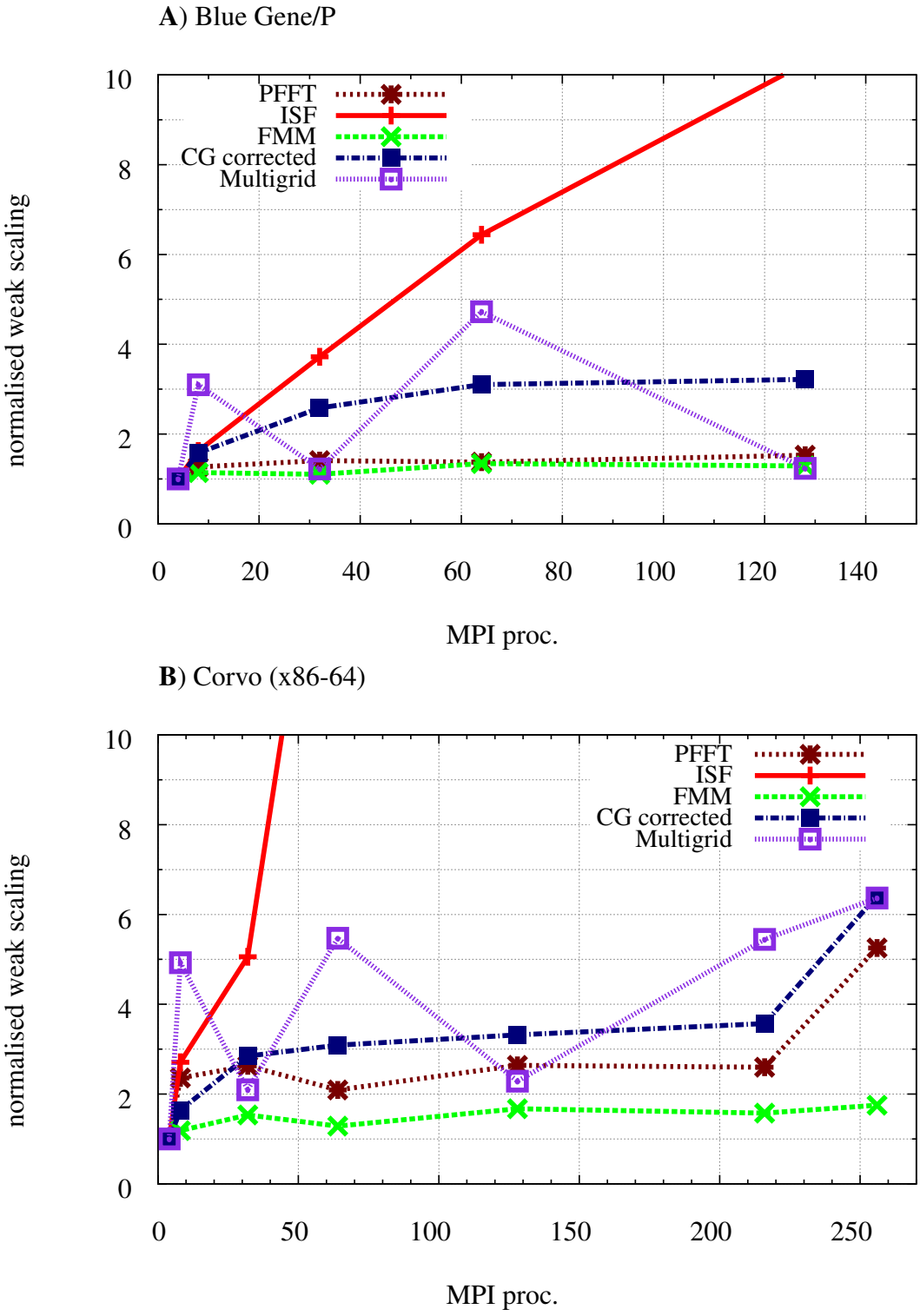

Figure 8: Normalised weak-scaling of the measured Poisson solvers in Blue Gene/P (A) and Corvo (B). Each MPI process has roughly 125,000 points and selected system sizes are given by L_e equal to 7.9, 10, 15.8, 20.1, 25.1 and 31.7 (the latter only in Corvo)

.

in the network of a Blue Gene/P machine than in that of a machine with x86-64 processors and Infiniband network (e.g. Corvo).

4.3 Influence of the input parameters

In this section we discuss several input parameters that we used in our tests of Poisson solvers. These parameters are the `BoxShape` (i.e., the spatial structure of the points where the Hartree potential was calculated), the `DeltaEFMM` (accuracy tolerance of the energy calculated with FMM), `MultigridLevels` (number of stages in the grid hierarchy of the multigrid solver) and `PoissonSolverMaxMultipole` (the order of the multipole expansion of the charges whose potential is analytically calculated when using multigrid or conjugate gradient solvers).

OCTOPUS is able to handle different grid shapes, like spherical, parallelepiped or *minimum* shapes (the *minimum* mesh shape is the addition of spheres centred in each nucleus of the test system). Apart from the mesh shape and size, the grid is defined by its spacing parameter, i.e., the distance between consecutive grid points. The *minimum* mesh shape option in OCTOPUS produces fair results with FMM. Serial FFT, PFFT, and ISF (which is based on FFT) solvers create a parallelepiped mesh —which contains the original minimum one— to calculate the Hartree potential. If multigrid or conjugate gradients are used with a minimum mesh, it is frequent to find a serious loss of accuracy. This is because minimal boxes are usually irregular, and the multipole expansion (whose terms are based on spherical harmonics, which are rather smooth) cannot adapt well to arbitrary charge values in irregular meshes[d]. These effects of box shape made us choose cubic meshes for our tests. In any case, one should take into account that if non-parallelepiped meshes are used, FMM suffers less overhead than the solvers based on reciprocal space (FFT, PFFT and ISF), since FMM can work directly with that data-representation and does not need to transfer data to a parallelepiped representation. Examples of this can be viewed in Table 3. There, it can be seen that the execution time is essentially the same regardless of the box shape for PFFT, while spherical and minimal box shapes are much more efficient than parallelepiped shape for FMM (with a ratio

[d]See the explanation of PoissonSolverMaxMultipole below for more information.

of about 1.67).

Spherical meshes are still valid for multigrid and conjugate gradient methods. We have compared the relative accuracy of cubic and spherical meshes for FMM, multigrid, and CG methods containing the same number of points. When FMM is used, both errors decrease while the mesh size is increased, being relatively equal for both representations, until an accuracy plateau is reached for big meshes. The same behaviour is shown for the multigrid solver and by the CG solver up to a given volume for a given system.

Table 3: Comparison of total times required for the calculation of the Hartree potential as a function of the box shape and radius (R) or semi-edge length (L_e) for PFFT and FMM solvers.

	PFFT			FMM		
$R \mid\mid L_e$(Å)	Minimal	Sphere	Parallelepiped	Minimal	Sphere	Parallelepiped
15.8	1.001	1.032	1.030	3.371	3.5413	5.945
22.1	2.535	2.6641	2.667	10.500	10.447	16.922
25.9	4.321	4.265	4.393	16.321	16.212	27.861
31.7	8.239	8.034	8.271	27.821	28.707	48.206

The implementations of multigrid and conjugate gradient solvers we used in our tests are based on a multipole expansion. Each value of the input charge density represented on a grid (ρ_{ijk}) is expressed with an analytic term via this multipole expansion, plus a numeric term. The Hartree potential created by the analytic part is calculated analytically, while the Hartree potential created by the numerical term is calculated numerically with either multigrid or conjugate gradient methods. Since the use of the analytic term makes the numerical term smaller, numerical errors are expected to be reduced. Therefore, the smaller the difference between the charge density and its multipole expansion, the smaller the potential numerically calculated (with multigrid or conjugate gradient solvers), and the higher the accuracy of the total Hartree potential calculation. An order for the multipole expansion (the input parameter `PoissonSolverMaxMultipole`, PSMM) must be chosen. It is to be stressed that arbitrarily higher values of PSMM do not lead to more accurate results; rather, there exists a PSMM that minimises the error for each problem. We ran some tests to obtain this optimal value. In them, we calculated the ground-state of a 180-atom chlorophyll

system using OCTOPUS, varying the value of PSMM. This molecule's size is expected to be large enough to be representative of a wide range of molecular sizes. The ground state calculations permit one to evaluate the final Hartree energy, as well as the HOMO-LUMO gap, which is defined as the difference between the highest occupied eigenvalue and the lowest unoccupied eigenvalue in a density functional theory calculation, and its value can be used for estimations of simulation accuracy.[84] Table 4 shows the obtained results. For $PSMM = 8, 9$, and 10, the accumulation of errors was big enough for calculations not to converge (this is because beyond a given order, the spherical harmonics are too steep to describe the ρ, which is rather smooth). From the data of Table 4, we chose $PSSM = 7$ for our simulations (with $PSSM = 7$ the HOMO-LUMO gap is equivalent to the reference value given by ISF, and the Hartree energy is the closest one).

Table 4: Ground state values of the Hartree energy and the HOMO-LUMO gap as a function of the PSMM (input parameter of Multigrid and Conjugate gradients solvers). Reference values are given by the ISF solver.

	Hartree energy (eV)			HOMO-LUMO gap		
PSMM	ISF	CG	Multigrid	ISF	CG	Multigrid
4	240821.47	240813.51	240813.41	1.4489	1.2179	1.2178
6	240821.47	240813.93	240813.95	1.4489	1.4340	1.4353
7	240821.47	240815.01	240814.69	1.4489	1.4520	1.4506

The implementation we used for FMM[47] allows one to tune the relative error of the calculations. Its expression is the quotient $(E_{ref} - E_n)/E_n$, i.e. the variable `DeltaEFMM`, where E_n is the Hartree energy calculated with the FMM method and E_{ref} is an estimation of what its actual value is. We chose for our calculations a relative error of 10^{-4}. Note that this error corresponds only to the pairwise term of the Hartree potential, before the correction for charge distribution (see section Section 2.3 and supporting info) is applied.

5 Conclusions

In this paper we analysed the relative performance of several popular methods (parallel fast Fourier transform, ISF, fast multipole method, conjugate gradients and multigrid) as implemented in the

OCTOPUS code for the calculation of the classical Hartree potential created by a charge distribution. The first part of the paper presents the fundamentals of these calculation methods. In the second part, we summarise the computational aspects of the tests we carried out to measure the methods' relative performances. These tests were run on three kinds of supercomputers, which we chose as representative of present-day high performance architectures. In the tests, we focused on measuring accuracies, execution times, speed-ups and weak-scalings. Test runs involved up to 4,096 parallel processes (each containing 4 OpenMP threads), and solved system sizes from about 350,000 grid points to about 32,000,000 grid points.

Our results (section Section 4) show that PFFT is the most efficient option when a high number of parallel processes are to be used. The current implementation of PFFT is very efficient, and should be the default option to study large physical systems using a number of cores beyond a certain threshold (when PFFT becomes faster than ISF). The fact that the charges are located at equispaced points makes FFT-based methods suitable for our problem. In special cases when charges are not lying in equispaced points (e.g. when curvilinear coordinates are used), FMM should be chosen instead, since it works and is accurate regardless of the charge density's spatial location. The FMM solver also shows good performance and scaling, yet its execution times are greater and its accuracy lower than those of the PFFT solver on the analysed machines. In contrast to ISF, FMM scales almost linearly up to high values of the number of processes, but since its numerical complexity has a larger prefactor, it would be competitive with ISF when the number of parallel processes increases significantly, a scenario in which the performance of ISF "collapses". The performance of the conjugate gradients solver has a trend similar to that of FMM, as does multigrid for low values of the number of processes. Weak-scaling tests show that communication overheads are the smallest for the FMM solver, while they are acceptable for PFFT, CG, and multigrid solvers, and they only significantly increases in the case of ISF, as we might expect from the data of Figure 5.

FFT-based methods (PFFT, serial FFT, and ISF) are more accurate than FMM, conjugate gradients, and multigrid. Hence, they should be chosen if accurate calculations of electrostatics are

required. However, according to our tests, the accuracy of all the analysed solvers is expected to be appropriate for density functional theory and time-dependent density functional theory calculations (where the calculation of the Hartree potential is an essential step) because these have other sources of error that will typically have a much stronger impact (section Section 4.1). Nevertheless, neither multigrid nor conjugate gradients can reach acceptable accuracy if the data set is not represented on a compact (spherical or parallelepiped) grid.

The competitive features of PFFT and FMM solvers make them suitable to perform calculations involving hundreds or thousands of processors to obtain electronic properties of large physical systems. ISF should be chosen only whenever a low number of parallel processes is to be used.

In the future, we plan to improve the accuracy and efficiency of the Poisson solvers implemented in OCTOPUS (keeping their suitability for both periodic boundaries and open systems) by taking advantage in the sparsity of the input data[85] and by including screened interactions (in the spirit of[86]).

Acknowledgement

We would like to express our gratitude to José Luis Alonso, Ivo Kabadshow and David Cardamone for support and illuminating advice. We acknowledge the PRACE Research Infrastructure resource Jugene based on Germany at Forschungszentrum Jülich and Curie based in France at CEA, funded by GENCI and the Rechenzentrum Garching (RZG) of the Max Planck Society for the usage of IBM Blue Gene/P. We specially acknowledge Laurent Nguyen for the support given for the Curie Supercomputer, Heiko Appel for the help given with the Genius supercomputer in Garching. We also acknowledge financial support from the European Research Council Advanced Grant DYNamo (ERC-2010-AdG-Proposal No. 267374), Spanish Grants (FIS2011-65702-C02-01 and PIB2010US-00652), ACI-Promociona (ACI2009-1036), general funding for research groups UPV/EHU (ALDAPA, GIU10/02), Grupos Consolidados UPV/EHU del Gobierno Vasco (IT-319-07) and European Commission project CRONOS (280879-2 CRONOS CP-FP7). P. García-Risueño is funded by the Humboldt Universität zu Berlin. J. Alberdi-Rodriguez acknowl-

edges the scholarship of the University of the Basque Country UPV/EHU. This work was partly supported by the BMBF under grant 01IH08001B.

Notes and References

(1) Hohenberg, P.; Kohn, W. *Phys. Rev.* **1964**, *136*, B864–B871.

(2) Kohn, W.; Sham, L. J. *Phys. Rev.* **1965**, *140*, A1133–A1138.

(3) Runge, E.; Gross, E. K. U. *Phys. Rev. Lett.* **1984**, *52*, 997–1000.

(4) Perdew, J. P.; Zunger, A. *Phys. Rev. B* **1981**, *23*, 5048–5079.

(5) Umezawa, N. *Phys. Rev. A* **2006**, *74*, 032505.

(6) Andrade, X.; Aspuru-Guzik, A. *Phys. Rev. Lett.* **2011**, *107*, 183002.

(7) Hartree, D. R. *The calculation of atomic structures*; J. Wiley: New York, 1957.

(8) Fock, V. A. *The Theory of space, time and gravitation*; Pergamon Press, 1964.

(9) Casida, M. E.; Jamorski, C.; Bohr, F.; Guan, J.; Salahub, D. R. In *Optical Properties from Density-Functional Theory*; American Chemical Society, 1996; Chapter 9, pp 145–163.

(10) García-Risueño, P.; Ibáñez, P. E. *International Journal of Modern Physics C (IJMPC)* **2012**, 1230001.

(11) Gygi, F.; Draeger, E. W.; Schulz, M.; de Supinski, B. R.; Gunnels, J. A.; Austel, V.; Sexton, J. C.; Franchetti, F.; Kral, S.; Ueberhuber, C. W.; Lorenz, J. Large-scale electronic structure calculations of high-Z metals on the BlueGene/L platform. *Proceedings of the 2006 ACM/IEEE conference on Supercomputing*, New York, NY, USA, 2006.

(12) Alonso, J. L.; Andrade, X.; Echenique, P.; Falceto, F.; Prada-Gracia, D.; Rubio, A. *Phys. Rev. Lett.* **2008**, *101*, 096403.

(13) Andrade, X.; Castro, A.; Zueco, D.; Alonso, J. L.; Echenique, P.; Falceto, F.; Rubio, A. *J. Chem. Theory Comput.* **2009**, *5*, 728–742.

(14) Andrade, X.; Alberdi-Rodriguez, J.; Strubbe, D. A.; Oliveira, M. J. T.; Nogueira, F.; Castro, A.; Muguerza, J.; Arruabarrena, A.; Louie, S. G.; Aspuru-Guzik, A.; Rubio, A.; Marques, M. A. L. *Journal of Physics: Condensed Matter* **2012**, *24*, 233202.

(15) Alberdi-Rodriguez, J. *Analysis of performance and scaling of the scientific code Octopus*; LAP LAMBERT Academic Publishing, 2010.

(16) Amdahl, G. M. Validity of the single processor approach to achieving large scale computing capabilities. *Proceedings of the April 18-20, 1967, spring joint computer conference*, New York, NY, USA, 1967; pp 483–485.

(17) Leach, A. R. *Molecular modelling: Principles and applications*, 2nd ed.; Pearson Education - Prentice Hall: Harlow, 2001.

(18) Tomasi, J.; Mennucci, B.; Cammi, R. *Chem. Rev.* **2005**, *105*, 2999–3094.

(19) Nayfeh, M. H.; Brussel, M. K. *Electricity and magnetism*; John Wiley & sons, 1985.

(20) Castro, A.; Rubio, A.; Stott, M. J. *Canadian Journal of Physics* **2003**, *81*, 1151–1164.

(21) Olivares-Amaya, R.; Stopa, M.; Andrade, X.; Watson, M. A.; Aspuru-Guzik, A. *The Journal of Physical Chemistry Letters* **2011**, *2*, 682–688.

(22) Watson, M. A.; Rappoport, D.; Lee, E. M. Y.; Olivares-Amaya, R.; Aspuru-Guzik, A. *The Journal of Chemical Physics* **2012**, *136*, 024101.

(23) Cooley, J. W.; Tukey, J. W. *Math. Comput.* **1965**, *19*, 297–301.

(24) Rozzi, C. A.; Varsano, D.; Marini, A.; Gross, E. K. U.; Rubio, A. *Phys. Rev. B* **2006**, *73*, 205119.

(25) Van Loan, C. *Computational frameworks for the fast Fourier transform*; Society for Industrial Mathematics, 1992; Vol. 10.

(26) Bluestein, L. I. *IEEE Trans AU* **1970**, *18*, 451–455.

(27) Ding, H. Q.; Gennery, D. B.; Ferraro, R. D. A Portable 3D FFT Package for Distributed-Memory Parallel Architectures. *Proceedings of 7th SIAM Conference on Parallel Processing*, 1995; pp 70–71.

(28) Eleftheriou, M.; Moreira, J. E.; Fitch, B. G.; Germain, R. S. A Volumetric FFT for BlueGene/L. *HiPC*, 2003; pp 194–203.

(29) Eleftheriou, M.; Fitch, B. G.; Rayshubskiy, A.; Ward, T. J. C.; Germain, R. S. *IBM Journal of Research and Development* **2005**, *49*, 457–464.

(30) Eleftheriou, M.; Fitch, B. G.; Rayshubskiy, A.; Ward, T. J. C.; Germain, R. S. Performance Measurements of the 3D FFT on the Blue Gene/L Supercomputer. *Euro-Par 2005 Parallel Processing*, 2005; pp 795–803.

(31) Pippig, M. *PFFT, Parallel FFT subroutine library*. `http://www.tu-chemnitz.de/~mpip`.

(32) Pippig, M. An Efficient and Flexible Parallel FFT Implementation Based on FFTW. *Competence in High Performance Computing*, 2010; pp 125–134.

(33) Pippig, M. *Preprint series of the Department of Mathematics, Chemnitz University of Technology* **2012**, *Preprint 2012-6*, 1–9.

(34) Plimpton, S. *Parallel FFT subroutine library*. `http://www.sandia.gov/~sjplimp/docs/fft/README.html`.

(35) Pekurovsky, D. *P3DFFT, Parallel FFT subroutine library*. `http://www.sdsc.edu/us/resources/p3dfft`.

(36) Li, N. *2DECOMP&FFT, Parallel FFT subroutine library*. `http://www.hector.ac.uk/cse/distributedcse/reports/incompact3d/incompact3d/index.html`.

(37) Truong Duy, T. V.; Ozaki, T. *ArXiv e-prints* **2012**, –.

(38) Frigo, M.; Johnson, S. G. *Proceedings of the* IEEE **2005**, *93*, 216–231.

(39) Genovese, L.; Deutsch, T.; Neelov, A.; Goedecker, S.; Beylkin, G. *Journal of Chemical Physics* **2006**, *125*, 074105, Genovese, L. and Deutsch, T. and Neelov, A. and Goedecker, S. and Beylkin, G.

(40) Genovese, L.; Neelov, A.; Goedecker, S.; Deutsch, T.; Ghasemi, S. A.; Willand, A.; Caliste, D.; Zilberberg, O.; Rayson, M.; Bergman, A.; Schneider, R. *The Journal of Chemical Physics* **2008**, *129*, 014109.

(41) Daubechies, I. *Ten Lectures on Wavelets*; SIAM, Philadelphia, PA, 1998.

(42) Goedecker, S. *Wavelets and their application for the solution of partial differential equations in physics*; Presses Polytechniques et Universitaires Romandes, 1998.

(43) Greengard, L. F.; Rokhlin, V. *J. Comp. Phys.* **1987**, *73*, 325–348.

(44) Greengard, L. F.; Rokhlin, V. *The Rapid Evaluation of Potential Fields in Three Dimensions*; Springer Press, Berlin, Heidelberg, 1988.

(45) Cheng, H.; Greengard, L. F.; Rokhlin, V. *J. Comp. Phys* **1999**, *155*, 468–498.

(46) Greengard, L. F.; Rokhlin, V. *Acta Numerica* **1997**, *6*, 229.

(47) Dachsel, H. *J. Chem. Phys.* **2010**, *132*, 119901.

(48) Cipra, B. A. *SIAM news* **2000**, *33, 4*, .

(49) White, C. A.; Johnson, B. G.; Gill, P. M. W.; Head-Gordon, M. *Chem. Phys. Lett.* **1994**, *230*, 8–16.

(50) White, C. A.; Johnson, B. G.; Gill, P. M. W.; Head-Gordon, M. *Chem. Phys. Lett.* **1996**, *253*, 268–278.

(51) Strain, M.; Scuseria, G.; Frisch, M. *Science* **1996**, *107*, 51–53.

(52) See supporting info.

(53) White, C. A.; Head-Gordon, M. *J. Chem. Phys.* **1994**, *101*, 6593–6605.

(54) Kabadshow, I.; Dachsel, H. The Error-Controlled Fast Multipole Method for Open and Periodic Boundary Conditions. *Fast Methods for Long-Range Interactions in Complex Systems*, Forschungszentrum Jülich, Germany, 2010.

(55) Saad, Y. *Iterative Methods for Sparse Linear Systems*; Society for Industrial and Applied Mathematics: Philadelphia, PA, USA, 2003.

(56) Chelikowsky, J. R.; Troullier, N.; Saad, Y. *Phys. Rev. Lett.* **1994**, *72*, 1240–1243.

(57) García-Risueño, P.; Echenique, P. *J. of Phys. A: Math. and Theor.* **2012**, *45*, 065204.

(58) Hestenes, M. R.; Stiefel, E. *J. of research of the national bureau of standards* **1952**, *49*, 409–436.

(59) Fernández-Serra, M. V.; Artacho, E.; Soler, J. M. *Phys. Rev. B* **2003**, *67*, 100101.

(60) Castro, A.; Appel, H.; Oliveira, M.; Rozzi, C.; Andrade, X.; Lorenzen, F.; Marques, M.; Gross, E.; Rubio, A. *Phys. Stat. Sol. B* **2006**, *243*, 2465–2488.

(61) Karypis, G.; Kumar, V. *SIAM Journal on Scientific Computing* **1998**, *20*, 359–392.

(62) Flocard, H.; Koonin, S. E.; Weiss, M. S. *Phys. Rev. C: Nucl. Phys.* **1978**, *17*, 1682–1699.

(63) Wesseling, P. *An introduction to multigrid methods*; John Wiley & Sons, 1992.

(64) Zhang, J. *J. Comp. Phys.* **1998**, *149*, 449–461.

(65) Briggs, W. L. *A multigrid tutorial*; Wiley, New York, 1987.

(66) Brandt, A. *Math. Comput* **1977**, *31*, 333–390.

(67) Trottenberg, U.; Oosterlee, C.; Schüller, A. *Multigrid*; Academic Press, 2001.

(68) Rostgaard, C.; Jacobsen, K. W.; Thygesen, K. S. *Phys. Rev. B* **2010**, *81*, 085103.

(69) Briggs, E. L.; Sullivan, D. J.; Bernholc, J. *Phys. Rev. B* **1996**, *54*, 14362–14375.

(70) Beck, T. T. *Rev. Mod. Phys.* **2000**, *72*, 1041.

(71) Torsti, T.; Heiskanen, M.; Puska, M. J.; Nieminen, R. M. *International Journal of Quantum Chemistry* **2003**, *91*, 171–176.

(72) Mortensen, J. J.; Hansen, L. B.; Jacobsen, K. W. *Phys. Rev. B* **2005**, *71*, 035109.

(73) Shapira, Y. *Matrix-Based Multigrid: Theory and Applications*; Numerical Methods and Algorithms; Kluwer Academic Publishers, 2003.

(74) Mandel, J.; McCormick, S. *Journal of Computational Physics* **1989**, *80*, 442–452.

(75) Marques, M. A. L.; Castro, A.; Bertsch, G. F.; Rubio, A. *Computer Physics Communications* **2003**, *151*, 60.

(76) Enkovaara, J. et al. *Journal of Physics: Condensed Matter* **2010**, *22*, 253202.

(77) Vila, F. D.; Strubbe, D. A.; Takimoto, Y.; Andrade, X.; Rubio, A.; Louie, S. G.; Rehr, J. J. *J. Chem. Phys.* **2010**, *133*, 034111.

(78) Fletcher, G. D.; Fedorov, D. G.; Pruitt, S. R.; Windus, T. L.; Gordon, M. S. *Journal of Chemical Theory and Computation* **2012**, *8*, 75–79.

(79) Jiang, W.; Hodoscek, M.; Roux, B. *Journal of Chemical Theory and Computation* **2009**, *5*, 2583–2588.

(80) Houzeaux, G.; de la Cruz, R.; Owen, H.; Vázquez, M. *Computers and Fluids* **2012**, –.

(81) Liu, Z.; Yan, H.; Wang, K.; Kuang, T.; Zhang, J.; Gui, L.; An, X.; Chang, W. *Nature* **2004**, *428*, 287–292.

(82) Goedecker, S.; Teter, M.; Hutter, J. *Phys. Rev. B* **1996**, *54*, 1703–1710.

(83) Definitions of basic concepts on high performance computing (e.g. 'node' and 'core') can be found in.[10]

(84) Wanko, M.; García-Risueño, P.; Rubio, Á. *physica status solidi (b)* **2012**, *249*, 392–400.

(85) Hassanieh, H.; Indyk, P.; Katabi, D.; Price, E. Nearly optimal sparse fourier transform. *Proceedings of the 44th symposium on Theory of Computing*, New York, NY, USA, 2012; pp 563–578.

(86) Cerioni, A.; Genovese, L.; Mirone, A.; Sole, V. A. *J. Chem. Phys.* **2012**, *137*, 134108.

Supporting info of: A survey of the parallel performance and the accuracy of Poisson solvers for electronic structure calculations

Pablo García-Risueño,[*,†] Joseba Alberdi-Rodriguez,[‡] Micael J. T. Oliveira,[¶] Xavier Andrade,[§] Michael Pippig,[‖] Javier Muguerza,[‡] Agustin Arruabarrena,[‡] and Ángel Rubio[⊥]

Humboldt Universität zu Berlin, University of the Basque Country UPV/EHU, University of Coimbra, Portugal, Harvard University, Chemnitz University of Technology, Germany, and European Theoretical Spectroscopy Facility and Fritz-Haber Institut (MPG), Germany

E-mail: risueno@physik.hu-berlin.de

Abstract

In this document, we include some information to complement our paper. First we provide some remarks on the way the data transfer for PFFT[1] and FMM[2] is carried out in our implementations. Then we add some remarks on the efficiency of the algorithms. Finally, we

[*]To whom correspondence should be addressed

[†]Institut für Physik, Humboldt Universität zu Berlin, 12489 Berlin, Germany

[‡]Dept. of Computer Architecture and Technology, Nano-Bio Spectroscopy Group and European Theoretical Spectroscopy Facility, Spanish node, University of the Basque Country UPV/EHU, M. Lardizabal, 1, 20018 Donostia/San Sebastián, Spain

[¶]Center for Computational Physics, University of Coimbra, Rua Larga, 3004-516 Coimbra, Portugal

[§]Dept. of Chemistry and Chemical Biology, 12 Oxford street, Cambridge, MA 02138, USA

[‖]Dept. of Mathematics, Chemnitz University of Technology, 09107 Chemnitz, Germany

[⊥]Nano-Bio Spectroscopy Group and European Theoretical Spectroscopy Facility, Spanish node, University of the Basque Country UPV/EHU, Edif. Joxe Mari Korta, Av. Tolosa 72, 20018 Donostia/San Sebastián, Spain - Centro de Física de Materiales, University of the Basque Country UPV/EHU, 20018 Donostia/San Sebastián, Spain - Fritz-Haber Institut der Max-Planck Gesellschaft, Faradayweg 4-6, D-14195 Berlin-Dahlem, Germany

discuss the correction term we devised to adapt the FMM method (originally devised to deal with point charges) to charge distributions.

For testing purposes we have used different portions of the chlorophyll molecule of the spinach photosynthetic unit,[3] that it is a quite remarkable and complex system. Our test systems consisted of 180, 441, 650 or 1365 atoms, and contained several chlorophyll units (see figure Figure S1). The space is represented with cubic grids with edge length $2L_e$ containing these molecules, where L_e is the half of the edge of the parallelepiped mesh and the used values are 15.8, 22.1, 25.9 and 31.7 respectively.

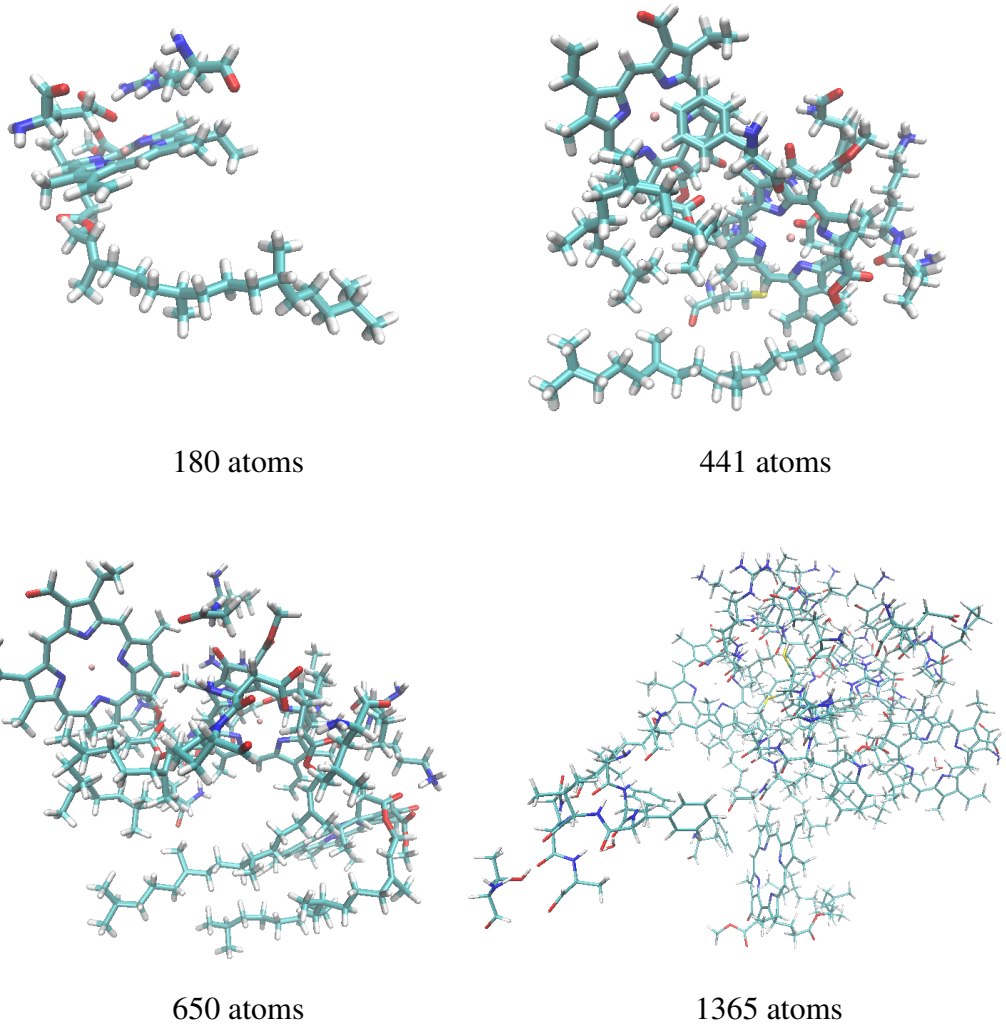

180 atoms 441 atoms

650 atoms 1365 atoms

Figure S1: Different chunks of the chlorophyll molecule of the spinach.

S1 Communication patterns

As stated in our paper, the way the data of variables is transferred from the main program (OCTOPUS in this case) and the Poisson solver can be critical for its efficiency. The data-transfer between the box used for PFFT and that one used by OCTOPUS (which contain different sets of points, see section 3 methods) has been encapsulated in an specific Fortran module. Each of those box representations corresponds to an MPI group. At a given moment, data points have to be send from one group (*sender I*) to the other (*receiver O*). Since both groups stores the same global grid, although in a different way, each point stored in a given process of one group is also stored in one process of the other group. For example, if point n is stored in process x_i of group I and in process y_o of group O, it should be sent from process x_i to process y_o. Unfortunately, MPI does not allow to send information between different groups unless they are disjoint, which is not the current case. This means communication will have to be done using only one of the groups (senders or receivers group). This is not a problem, because we can determine the rank of the receiver process in the I group through the rank in the `MPI_COMM_WORLD` global communicator. Then, point n is sent from process x_i to process y_i.

We have implemented a routine that determines to which process each point should be sent. This information is then used to put the data in the "correct order". Then, a simple call to the `MPI_Alltoall` function is enough for the communication step. It is important to note that, using this technique, each process only transfers each point once. Therefore, the total amount of information that must be sent between all the processes is equal to the number of points in the grid, and it is independent of the number of processes.

The PFFT library requires two communication steps in addition to the box transformation. Required communication needs are two `MPI_Alltoall` calls for every calculated FFT. In total, six `MPI_Alltoall` calls are needed in every Poisson solver.

Regarding to the FMM library, three MPI global communication functions have to be executed: `MPI_Allgather`, `MPI_Allreduce` and `MPI_Alltoall`. Additionally, synchronization between different FMM levels has to be done using `MPI_Barrier`.[4]

S2 More comments on execution-time

Our tests showed that the novel implementations of PFFT[5] and FMM[2] offer a good scalability and accuracy, and are competitive if thousands of parallel processes are available. Figure S2 shows the speed-ups obtained using PFFT for the different system sizes in a BlueGene/P supercomputer. Almost linear performances can be observed until saturation for all the cases, and the obtained efficiencies have been always above 50% for just nearly all these points. As expected, large systems, which have higher computation needs, can make a better use of a high number of processes. Tests run in Corvo and Curie machines show similar trends (although with efficiency problems of PFFT for some values of MPI proc.).

S3 Correction terms for FMM

S3.1 General remarks

The fast multipole method (FMM)[2,6–9] was devised to efficiently calculate pairwise potentials created by pointlike charges, like pairwise Coulomb potential. In the literature it is possible to find some modifications of the traditional FMM which deal with charges which are modelled as Gaussian functions.[10] Such modifications of FMM can be used into LCAO codes as Gaussian[11] or FHI-Aims. However, they are not useful when the charge distribution is represented through a set of discrete charge density values. The Fast Multipole Method presented in[2,12] belongs to the family of FMM methods which calculate the electrostatic potential created by a set of pointlike charges. This method is very accurate and efficient, but it needs some modifications to work in programs like OCTOPUS,[13,14] where the 3D grid points actually represent charge densities. As stated in the section 'Theoretical background' of the paper, the electronic density is a $\mathbb{R}^3 \rightarrow \mathbb{R}$ field, where values of the $\mathbb{R}^3$ set correspond to a equispaced grid (see Figure S3 C)). The variable $\rho_{j,k,l}$ is the charge density at the portion of volume (cell) centred in the point (j,k,l). Each cell is limited by the planes bisecating the lines that join two consecutive grid points, and its volume is

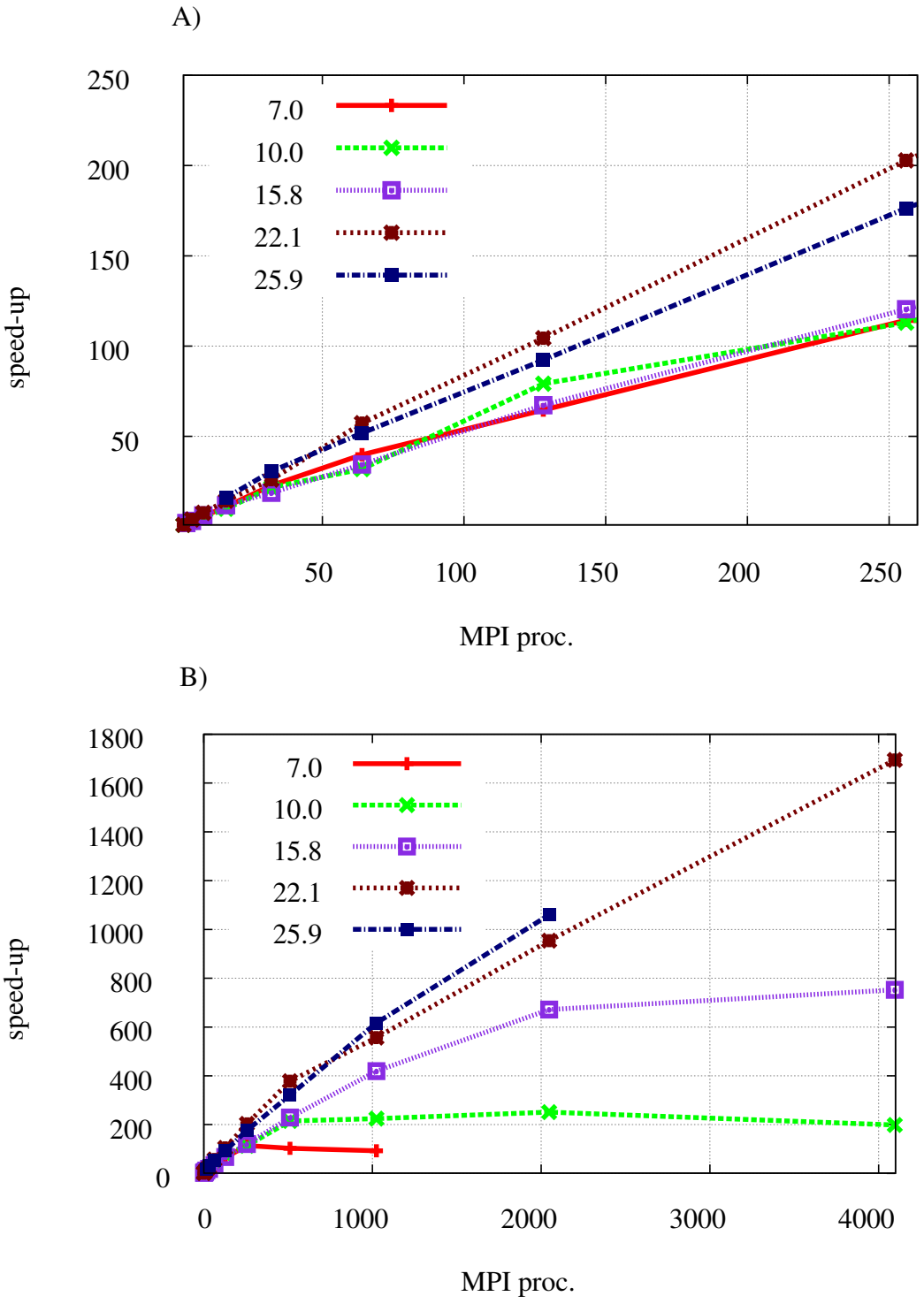

Figure S2: Speed-up of the PFFT Poisson solver in a Blue Gene/P computer for different system sizes (given by L_e, semi-legth of the parallelepiped edge). Largest systems saturate with more processes than the smallers ones. A) linear speed-up is shown up to 256 processes, independently of the simulated system. B) saturation point is higher when the simulated system is bigger.

$\Omega = L^3$, being L the spacing between consecutive grid points. The density $\rho_{j,k,l}$ is always negative and it is expected to vary slowly among nearby points.

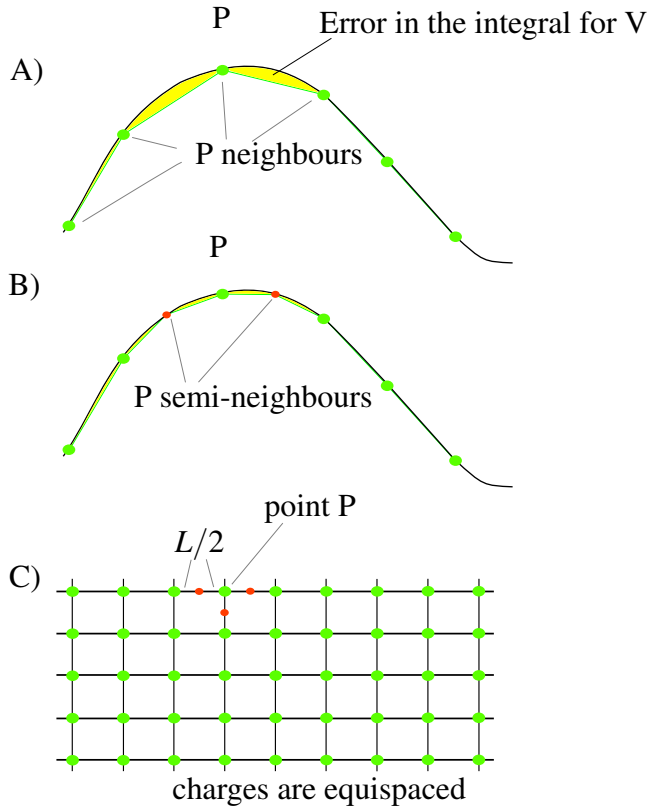

Figure S3: Scheme of how the inclusion of semi-neighbours of point P (pink points) helps to improve the accuracy of the integration to calculate the Hartree potential. A) Scheme of the function whose integration will be approximated by a summation, without considering semi-neighbours. B) id., considering semi-neighbours of point P; The error made by the approximation is proportional to the yellow surface in A) and B). C) 2D scheme of the grid: green points are grid points, while pink points are semi-neighbours of P.

The term v^{SI} in equation 16 of the paper can be calculated analytically as follows assuming that the cell is a sphere of volume Ω:

$$\begin{aligned} v^{\mathrm{SI}}(\vec{r}_0) &= \int_\Omega d\vec{r}\frac{\rho(\vec{r})}{|\vec{r}-\vec{r}_0|} = \rho(\vec{r}_0)\int_\Omega d\vec{r}\frac{1}{|\vec{r}-\vec{r}_0|} \\ &\simeq \rho(\vec{r}_0)\int_0^R dr\int_0^{2\pi} d\phi\int_0^{\pi} d\theta\frac{r^2 sen(\theta)}{r} \\ &= \rho(\vec{r}_0)2\pi L^2\left(\frac{3}{4\pi}\right)^{2/3}, \end{aligned} \tag{1}$$

where we have used the approximation of constant charge density within the cell. One may expect this approximate way to proceed to be less accurate than the numerical integration of $1/r$ in a cubic cell (what is also efficient, since the integration through an arbitrary size cube is proportional to the integral through a cube of unit volume). However, it happens the converse: the difference between both methods is small (about 1% of difference between integrals) but, due to error cancellations, the analytical method is slightly more accurate when calculating potentials.

The term $v^{\text{corr.}}_{j,k,l}$ in (equation 16) is included to calculate more accurately the potential created by the charge in cells nearby to (j,k,l). To devise a expression for it, we consider that charge distribution is similar to sets of Gaussians centred in the atoms of the system. For Gaussian distributions, the greatest concavity near the centre of the Gaussian makes the influence of neighbouring points to be major for the potential. As we can see in the scheme of Figure S3 A)-B), considering semi-neighbours of point P (in $\vec{r}_0 := (j,k,l)$), i.e., points whose distance to P is not L, but $L/2$, the integral of equation 16 of the paper can be calculated in a much more accurate way.

S3.2 Method 1: 6-neighbours correction

We build a corrective term by calculating the charge in the 6 semi-neighbours of every point of the mesh $\vec{r}_0$ (see Figure S4 for a intuitive scheme). The total correction term is the potential created by the semi-neighbours ($v^{\text{corr.}+}$) minus the potential created by the charge lying in the volume of the semi-neighbour cells that was already counted in v^{FMM} or in v^{SI} ($v^{\text{corr.}-}$):

$$v^{\text{corr.}}(\vec{r}_0) = v^{\text{corr.}+}(\vec{r}_0) - v^{\text{corr.}-}(\vec{r}_0)\ . \tag{2}$$

In order to calculate $v^{\text{corr.}+}$, we use the formula por the 3rd degree interpolation polynomial:

$$f(0) = \frac{(-1)}{16} f\left(\frac{-3}{2}L\right) + \frac{9}{16} f\left(\frac{-L}{2}\right) + \frac{9}{16} f\left(\frac{L}{2}\right) - \frac{(-1)}{16} f\left(\frac{3}{2}L\right) \ , \tag{3a}$$

$$f\left(\frac{-L}{2}\right) = \frac{(-1)}{16} f(-2L) + \frac{9}{16} f(-L) + \frac{9}{16} f(0) - \frac{(-1)}{16} f(L) \ , \tag{3b}$$

$$f\left(\frac{L}{2}\right) = \frac{(-1)}{16} f(-L) + \frac{9}{16} f(0) + \frac{9}{16} f(L) - \frac{(-1)}{16} f(2L) \ . \tag{3c}$$

So, the semi-neighbours of $\vec{r}_0 = (x_0, y_0, z_0)$ are

$$\begin{aligned}
\rho(x_0 - L/2, y_0, z_0) =& \frac{-1}{16}\rho(x_0 - 2L, y_0, z_0) + \frac{9}{16}\rho(x_0 - L, y_0, z_0) \\
&+ \frac{9}{16}\rho(x_0, y_0, z_0) - \frac{1}{16}\rho(x_0 + L, y_0, z_0) \ ; \qquad (4a) \\
\rho(x_0 + L/2, y_0, z_0) =& \frac{-1}{16}\rho(x_0 - L, y_0, z_0) + \frac{9}{16}\rho(x_0, y_0, z_0) \\
&+ \frac{9}{16}\rho(x_0 + L, y_0, z_0) - \frac{1}{16}\rho(x_0 + 2L, y_0, z_0) \ ; \qquad (4b) \\
\rho(x_0, y_0 - L/2, z_0) =& \frac{-1}{16}\rho(x_0, y_0 - 2L, z_0) + \frac{9}{16}\rho(x_0, y_0 - L, z_0) \\
&+ \frac{9}{16}\rho(x_0, y_0, z_0) - \frac{1}{16}\rho(x_0, y_0 + L, z_0) \ ; \qquad (4c) \\
\rho(x_0, y_0 + L/2, z_0) =& \frac{-1}{16}\rho(x_0, y_0 - L, z_0) + \frac{9}{16}\rho(x_0, y_0, z_0) \\
&+ \frac{9}{16}\rho(x_0, y_0 + L, z_0) - \frac{1}{16}\rho(x_0, y_0 + 2L, z_0) \ ; \qquad (4d) \\
\rho(x_0, y_0, z_0 - L/2) =& \frac{-1}{16}\rho(x_0, y_0, z_0 - 2L) + \frac{9}{16}\rho(x_0, y_0, z_0 - L) \\
&+ \frac{9}{16}\rho(x_0, y_0, z_0) - \frac{1}{16}\rho(x_0, y_0, z_0 + L) \ ; \qquad (4e) \\
\rho(x_0, y_0, z_0 + L/2) =& \frac{-1}{16}\rho(x_0, y_0, z_0 - L) + \frac{9}{16}\rho(x_0, y_0, z_0) \\
&+ \frac{9}{16}\rho(x_0, y_0, z_0 + L) - \frac{1}{16}\rho(x_0, y_0, z_0 + 2L) \ . \qquad (4f)
\end{aligned}$$

We consider all this six charges to be homogeneously distributed in cells whose volume is $\Omega/8$. The distance between the centre of these small cells and the centre of the cell whose v we are

calculating (i.e., the cell centred in $\vec{r}_0$) is $L/2$. So the first part of $v^{\text{corr.}}(\vec{r}_0)$ is

$$\begin{aligned} v^{\text{corr.}+}(\vec{r}_0) &= \Big(\rho(x_0-L/2,y_0,z_0)+\rho(x_0+L/2,y_0,z_0)+\ldots+ \\ &+ \rho(x_0,y_0,z_0+L/2)\Big)\left(\frac{\Omega}{8}\right)\left(\frac{1}{L/2}\right) . \end{aligned} \tag{5}$$

Since we have created these new 6 cells, we must subtract the potential created by their corresponding volume from that created by the cells whose volume is partly occupied by these new cells. This potential is:

$$\begin{aligned} v^{\text{corr.}-}(\vec{r}_0) &= \Big(\rho(x_0-L,y_0,z_0)+\rho(x_0+L,y_0,z_0)+\rho(x_0,y_0-L,z_0)+\rho(x_0,y_0+L,z_0) \\ &+ \rho(x_0,y_0,z_0-L)+\rho(x_0,y_0,z_0+L)\Big)\left(\frac{\Omega}{16}\right)\left(\frac{1}{L}\right)+\alpha\, v^{\text{SI}}(\vec{r}_0) . \end{aligned} \tag{6}$$

The aim of the term $\alpha\, v^{\text{SI}}$ (i.e., the variable `AlphaFMM` in OCTOPUS) is to compensate the errors arising from the assumption that the charge is concentrated at the centre of the cells and reduced cells. The value of α is tuned to minimize the errors in the potentials.

It is worth to re-express as follows the correction terms of eqs. Eq. (2), Eq. (4f) and Eq. (4f) avoiding to call to every variable more than once for the sake of getting higher computational efficiency:

$$\begin{aligned} v^{\text{SI}}(\vec{r}_0)+v^{\text{corr.}}(\vec{r}_0) = L^2\Big[& \rho(x_0,y_0,z_0)\big(27/32+(1-\alpha)2\pi(3/4\pi)^{2/3}\big) \\ & +(1/16)\Big(\rho(x_0-L,y_0,z_0)+\rho(x_0+L,y_0,z_0)+\rho(x_0,y_0-L,z_0) \\ & +\rho(x_0,y_0+L,z_0)+\rho(x_0,y_0,z_0-L)+\rho(x_0,y_0,z_0+L) \\ & -(1/4)\big(\rho(x_0-2L,y_0,z_0)+\rho(x_0+2L,y_0,z_0)+\rho(x_0,y_0-2L,z_0) \\ & +\rho(x_0,y_0+2L,z_0)+\rho(x_0,y_0,z_0-2L)+\rho(x_0,y_0,z_0+2L)\big)\Big)\Big] . \end{aligned} \tag{7}$$

A)

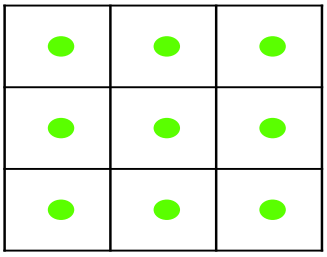

Original box: all cell's size is L^2 (2D)

B)

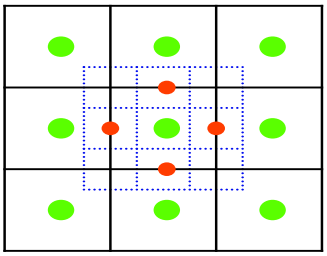

New: Semi-neighbours cell sizes are $L^2/4$

Side cells sizes are $7/8L^2$

Central cell size is $L^2/2$

(all in 2D)

Figure S4: 2D example of the position of cells containing semi neighbours. Assume the centre of the plots is $\vec{r}_0$, the point where we want to calculate the correcting term for the potential. The volume of semi-neighbour cells is $L^2/4$ in 2D, and $\Omega/8$ in 3D. One half of the semi-neighbour cell occupies the volume of a neighbour cell (the cell whose centre is L away from $\vec{r}_0$). The other half of the semi-neighbour cell occupies the space of the $\vec{r}_0$-centred cell itself.

We ran tests using the error formula $E := \sqrt{\sum_i (v^{\text{Exact}}(\vec{r}_i) - v^{\text{FMM}}(\vec{r}_i))^2}$, with the index i running for all points of the system. The inclusion of the correcting term introduced in this section typically reduced E in a factor about 50.

S3.3 Method 2: 124-neighbours correction

This method is similar to the one explained in the previous section, but with two differences

- It uses 3D interpolation polynomials, instead of 1D polynomials. Then, it considers $5^3 - 1 = 124$ neighbours in a cube of edge $5L$ centred in $\vec{r}_0$ to calculate the corrective term for $V(\vec{r}_0)$
- The interpolation polynomials representing $\rho(x,y,z)$ are numerically integrated (after their division by r). This is, we calculate

$$v^{\text{corr.}+}(\vec{r}_0) = \int_{125\Omega} d\vec{r} \frac{\rho(\vec{r})}{|\vec{r}-\vec{r}_0|} \simeq \int_{125\Omega} d\vec{r} \frac{Pol(\vec{r})}{|\vec{r}-\vec{r}_0|} . \quad (8)$$

The integration is to be performed between -5/2L and 5/2L for x, y and z. The interpolation polynomial (with 125 support points) $Pol(\vec{r})$ is

$$Pol(\vec{r}) = \sum_{i=1}^{5}\sum_{j=1}^{5}\sum_{k=1}^{5} \rho(x_0+(i-3)L, y_0+(j-3)L, z_0+(k-3)L)\alpha_i(x)\alpha_j(y)\alpha_k(z) \ , \tag{9}$$

being

$$\alpha_1(\xi) := \frac{\xi^4}{24} - \frac{\xi^3}{12} - \frac{\xi^2}{24} + \frac{\xi}{12} \ , \tag{10a}$$

$$\alpha_2(\xi) := -\frac{\xi^4}{6} + \frac{\xi^3}{6} + \frac{2\xi^2}{3} - \frac{2\xi}{3} \ , \tag{10b}$$

$$\alpha_3(\xi) := \frac{\xi^4}{4} - \frac{5\xi^2}{4} + 1 \ , \tag{10c}$$

$$\alpha_4(\xi) := -\frac{\xi^4}{6} - \frac{\xi^3}{6} + \frac{2\xi^2}{3} + \frac{2\xi}{3} \ , \tag{10d}$$

$$\alpha_5(\xi) := \frac{\xi^4}{24} + \frac{\xi^3}{12} - \frac{\xi^2}{24} - \frac{\xi}{12} \ . \tag{10e}$$

The quotient of the polynomials $\alpha_i(x)\alpha_j(y)\alpha_k(z)$ divided by $|\vec{r}-\vec{r}_0|$ can be numerically integrated through the cubic cell of edge 5L and centred in x_0. Such integrals can indeed be tabulated, because equation (Section S3.3) implies $v^{\text{corr.}+}(\vec{r}_0) = v^{\text{corr.}+}(\vec{r}_0)|_{L=1} \cdot L^2$. Terms of $\alpha_i(x)\alpha_j(y)\alpha_k(z)/|\vec{r}-\vec{r}_0|$ are often odd functions whose integral is null. The non-zero integrals taking part in (Figure S3) (with $L = 1$) can be easily calculated numerically.

Therefore

$$
\begin{aligned}
v^{\mathrm{corr.}+}(\vec{r}_0) &= \sum_{i=1}^{5}\sum_{j=1}^{5}\sum_{k=1}^{5} \rho(x_0+(i-3)L, y_0+(j-3)L, z_0+(k-3)L)\cdot \\
&\quad \int_{125\Omega} d\vec{r} \frac{\alpha_i(x)\alpha_j(y)\alpha_k(z)}{|\vec{r}-\vec{r}_0|} \\
&= \sum_{i=1}^{5}\sum_{j=1}^{5}\sum_{k=1}^{5} \rho(x_0+(i-3)L, y_0+(j-3)L, z_0+(k-3)L)\cdot \\
&\quad \sum_{l=1}^{5}\sum_{m=1}^{5}\sum_{n=1}^{5} \alpha_{i,l}\alpha_{j,m}\alpha_{k,n} \int_{125\Omega} d\vec{r} \frac{x^{l-1}y^{m-1}z^{n-1}}{|\vec{r}-\vec{r}_0|} \\
&= \sum_{i=1}^{5}\sum_{j=1}^{5}\sum_{k=1}^{5} \rho(x_0+(i-3)L, y_0+(j-3)L, z_0+(k-3)L)\cdot \\
&\quad \sum_{l=1}^{5}\sum_{m=1}^{5}\sum_{n=1}^{5} \alpha_{i,l}\alpha_{j,m}\alpha_{k,n}\beta(l-1,m-1,n-1)L^2 \,, \qquad (11)
\end{aligned}
$$

where $\alpha_{i,l}$ is the coefficient of ξ^{l-1} if $\alpha_i(\xi)$ and

$$
\beta(l,m,n) := \int_{-1/2}^{1/2} dx \int_{-1/2}^{1/2} dy \int_{-1/2}^{1/2} dz \frac{x^l y^m z^n}{\sqrt{x^2+y^2+z^2}} \,. \qquad (12)
$$

In this case, $v^{\mathrm{corr.}-}$ is equal to all the contributions to $V(\vec{r}_0)$ due to charges whose position (x,y,z) satisfies

$$
|x-x_0| <= 2L;\ |y-y_0| <= 2L;\ |z-z_0| <= 2L \,, \qquad (13)
$$

including self-interaction integral.

This way to calculate $v^{\mathrm{corr.}+}$ is not inefficient, because only 27 integrals are not null, and both α and β are known. In order to calculate $v^{\mathrm{corr.}+}(\vec{r}_0)$ we need 125 products and additions, what is essentially the same number of operations which is required in order to calculate the potential created in $\vec{r}_0$ by the neighbouring points (whose calculation can be removed and then saved). Nevertheless, results using this correction method were worse than that obtained using the first method, so only that one was implemented into the standard version of OCTOPUS.

References

(1) Pippig, M. *PFFT, Parallel FFT subroutine library*. `http://www.tu-chemnitz.de/~mpip`.

(2) Dachsel, H. *J. Chem. Phys.* **2010**, *132*, 119901.

(3) Liu, Z.; Yan, H.; Wang, K.; Kuang, T.; Zhang, J.; Gui, L.; An, X.; Chang, W. *Nature* **2004**, *428*, 287–292.

(4) Kabadshow, I.; Dachsel, H.; Hammond, J. Poster: Passing the three trillion particle limit with an error-controlled fast multipole method. *Proceedings of the 2011 companion on High Performance Computing Networking, Storage and Analysis Companion*, New York, NY, USA, 2011; pp 73–74.

(5) Pippig, M. *Preprint series of the Department of Mathematics, Chemnitz University of Technology* **2012**, *Preprint 2012-6*, 1–9.

(6) Greengard, L. F.; Rokhlin, V. *J. Comp. Phys.* **1987**, *73*, 325–348.

(7) Greengard, L. F.; Rokhlin, V. *The Rapid Evaluation of Potential Fields in Three Dimensions*; Springer Press, Berlin, Heidelberg, 1988.

(8) Greengard, L. F.; Rokhlin, V. *Acta Numerica* **1997**, *6*, 229.

(9) Cheng, H.; Greengard, L. F.; Rokhlin, V. *J. Comp. Phys* **1999**, *155*, 468–498.

(10) Strain, M.; Scuseria, G.; Frisch, M. *Science* **1996**, *107*, 51–53.

(11) Frisch, M. J. et al. *Gaussian 09 Revision A.1*, 2009. `www.gaussian.com`, Gaussian Inc. Wallingford CT 2009.

(12) Kabadshow, I.; Dachsel, H. The Error-Controlled Fast Multipole Method for Open and Periodic Boundary Conditions. *Fast Methods for Long-Range Interactions in Complex Systems*, Forschungszentrum Jülich, Germany, 2010.

(13) Castro, A.; Appel, H.; Oliveira, M.; Rozzi, C.; Andrade, X.; Lorenzen, F.; Marques, M.; Gross, E.; Rubio, A. *Phys. Stat. Sol. B* **2006**, *243*, 2465–2488.

(14) Marques, M. A. L.; Castro, A.; Bertsch, G. F.; Rubio, A. *Computer Physics Communications* **2003**, *151*, 60.